

HPPP: Halpern-type Preconditioned Proximal Point Algorithms and Applications to Image Restoration*

Shuchang Zhang[†], Hui Zhang[‡], and Hongxia Wang[§]

Abstract. Recently, the degenerate preconditioned proximal point (PPP) method provided a unified and flexible framework for designing and analyzing operator-splitting algorithms, such as the Douglas-Rachford (DR) splitting. However, the degenerate PPP method exhibits weak convergence in the infinite-dimensional Hilbert space and lacks accelerated variants. To address these issues, we propose a Halpern-type PPP (HPPP) algorithm, which leverages the strong convergence and acceleration properties of Halpern’s iteration method. Moreover, we propose a novel algorithm for image restoration by combining HPPP with denoiser priors, such as the Plug-and-Play (PnP) prior, which can be viewed as an accelerated PnP method. Finally, numerical experiments, including several toy examples and image restoration, validate the effectiveness of our proposed algorithms.

Key words. Halpern iteration, preconditioned proximal point algorithms, Plug-and-Play Prior, regularization by denoising, image restoration

1. Introduction. Image restoration (IR) problems, including image deblurring, super-resolution, and inpainting, can be formulated as the following optimization problem [16, 27]:

$$(1.1) \quad \min_{\mathbf{x} \in \mathcal{X}} \lambda f(\mathbf{x}) + g(\mathbf{K}\mathbf{x}),$$

where $f : \mathcal{X} \rightarrow \mathbb{R} \cup \{+\infty\}$ and $g : \mathcal{Y} \rightarrow \mathbb{R} \cup \{+\infty\}$ are convex, lower semicontinuous functions, $\mathbf{K} : \mathcal{X} \rightarrow \mathcal{Y}$ is a bounded linear operator, and $\lambda > 0$ is a balance parameter. Both \mathcal{X} and \mathcal{Y} are real Hilbert spaces. The first term f represents the data fidelity, while the second term g serves as a regularization, such as TV (total variation) [48], to mitigate the ill-posedness of IR problems.

By the first-order optimality condition, the convex optimization problem (1.1) is equivalent to the following inclusion problem:

$$(1.2) \quad \text{find } \mathbf{x} \in \mathcal{X} \text{ such that } \mathbf{0} \in \lambda \partial f(\mathbf{x}) + \mathbf{K}^* \partial g(\mathbf{K}\mathbf{x}),$$

where $\partial f(\mathbf{x})$ and $\partial g(\mathbf{x})$ are the subdifferentials of f and g at \mathbf{x} , respectively [5, Chapter 3]. Following [27, 9], by introducing an auxiliary variable $\mathbf{y} \in \partial g(\mathbf{K}\mathbf{x})$, we reformulate (1.2) as

$$(1.3) \quad \text{find } \mathbf{u} \in \mathcal{H} \text{ such that } \mathbf{0} \in \mathcal{A}\mathbf{u},$$

***Funding:** This work was supported by the National Key Research and Development Program (2020YFA0713504) and the National Natural Science Foundation of China (grants 12471300 and 12471401).

[†]Department of Mathematics, National University of Defense Technology, Changsha, 410073, China (zhang-shuchang19@nudt.edu.cn).

[‡]Department of Mathematics, National University of Defense Technology, Changsha, 410073, China (h.zhang1984@163.com).

[§]Corresponding author. Department of Mathematics, National University of Defense Technology, Changsha, 410073, China (wanghongxia@nudt.edu.cn).

where $\mathcal{A} = \begin{pmatrix} \lambda \partial f & \mathbf{K}^* \\ -\mathbf{K} & (\partial g)^{-1} \end{pmatrix}$, $\mathbf{u} = (\mathbf{x}, \mathbf{y})$, and $\mathcal{H} = \mathcal{X} \times \mathcal{Y}$. The problem (1.3) is common in modern optimization and variational analysis [2, 3]. When \mathcal{A} is maximal monotone, the resolvent $J_{\mathcal{A}} = (I + \mathcal{A})^{-1}$ is nonexpansive with a full domain, as established by the Minty surjectivity theorem [39]. The proximal point iteration $\mathbf{u}^{k+1} = (I + \mathcal{A})^{-1} \mathbf{u}^k$ is used to solve (1.3) and converges weakly [46]. However, it is difficult to compute the operator $(I + \mathcal{A})^{-1}$, and hence splitting methods have been developed to address this issue. The well-known Douglas-Rachford splitting (DRS) [23] decomposes \mathcal{A} into the sum of two maximal monotone operators \mathcal{A}_1 and \mathcal{A}_2 , for which $J_{\mathcal{A}_1}$ and $J_{\mathcal{A}_2}$ are easier to obtain. Another way to solve (1.1) is to transform it into a saddle-point problem [16, 43], i.e.,

$$(1.4) \quad \min_{\mathbf{x} \in \mathcal{X}} \max_{\mathbf{y} \in \mathcal{Y}} \langle \mathbf{K}\mathbf{x}, \mathbf{y} \rangle + \lambda f(\mathbf{x}) - g^*(\mathbf{y}),$$

where $g^* : \mathcal{Y} \rightarrow \mathbb{R} \cup \{+\infty\}$ is the conjugate of g . In this direction, many primal-dual methods, including the well-known Chambolle-Pock (CP) primal-dual method [16, 43] and the primal-dual hybrid gradient (PDHG) method [27], are designed and studied extensively. In particular, He and Yuan [27] analyzed the PDHG method from a PPP standpoint with a positive definite preconditioner $\mathcal{M} : \mathcal{H} \rightarrow \mathcal{H}$. Recently, Bredies et al. [11, 12, 9] developed a unified degenerate PPP algorithmic framework with a positive semidefinite \mathcal{M} . By choosing appropriate preconditioners, this framework could cover the DR and CP algorithms [9].

It is crucial to study algorithms that exhibit both strong convergence and acceleration [30, 8, 34, 3, 52, 17, 38], such as strongly convergent proximal point methods [30] and forward-reflected-backward splitting algorithms [34]. For example, Bauschke et al. demonstrated strong convergence of degenerate PPP under the special case where \mathcal{A} is linear [3]. In such cases, the weak limit of the PPP sequence corresponds to the \mathcal{M} -projection of the initial point. Moreover, Sun et al. [52] proposed an accelerated preconditioned alternating direction method of multipliers (pADMM) by leveraging the degenerate PPP method [9] and the fast Krasnosel'skiĭ-Mann (KM) iteration [6]. Similarly, Chen et al. introduced an accelerated HPR-LP solver, which implements a Halpern Peaceman-Rachford method enhanced with semiproximal terms for efficiently solving linear programming (LP) problems [17], and the restarted Halpern PDHG (rHPDHG) achieves an accelerated linear convergence rate [38]. A shortcoming of forward-backward and DRS algorithms employing KM iteration is that their iterates converge only in the weak topology [8]. Consequently, the degenerate PPP method based on KM iteration typically exhibits weak convergence in Hilbert spaces. Meanwhile, it is unclear whether the degenerate PPP method can be accelerated via simple modification.

The classic Halpern iteration [26] offers the advantage of strong convergence over the KM iteration in infinite-dimensional Hilbert spaces, with the limit identified as the metric projection of the anchor onto the fixed point set [29]. Then the Halpern iteration is also known as an implicitly regularized method [22]. Due to this implicit regularity, the degenerate PPP method incorporating Halpern iteration can obtain a unique solution, yielding stable recovery results for IR problems. Achieving stable reconstruction for ill-posed inverse problems is important [24]. Moreover, beyond the implicit regularity, Halpern iteration can also accelerate convergence rate in terms of operator residual norm [55], which is widely utilized in machine learning [22, 41, 29]. Notably, the work [41] has demonstrated that PDHG with restarted

Halpern iteration achieves a faster convergence rate for function values in CT image reconstruction. Based on the Halpern iteration, the following Halpern-type preconditioned proximal point algorithm (called HPPP) (1.5) is thus proposed to overcome the two limitations of the degenerate PPP method:

$$(1.5) \quad \mathbf{u}^{k+1} = \mu_{k+1} \mathbf{a} + (1 - \mu_{k+1}) \mathcal{T} \mathbf{u}^k,$$

where $\mathcal{T} = (\mathcal{A} + \mathcal{M})^{-1} \mathcal{M}$, and \mathcal{A}, \mathcal{M} are detailed in subsection 3.3, and $\mathbf{a}, \mathbf{u}^0 \in \mathcal{H}$ are the anchor point and the initial point, respectively, and $\{\mu_k\}_{k \in \mathbb{N}}$ is a sequence in $[0, 1]$ such that $\sum_{k \in \mathbb{N}} \mu_k = +\infty, \lim_{k \rightarrow \infty} \mu_k = 0$.

PnP (Plug-and-Play) methods that combine splitting algorithms with denoiser priors have been widely applied in practical problems [56, 51, 1, 35, 59] and have achieved state-of-the-art performance in inverse imaging tasks [65, 33, 53]. Buzzard et al. provided a consensus equilibrium interpretation on denoiser priors [14]. Romano, Elad, and Milanfar introduced RED (regularization by denoising) [47], whose gradient exactly corresponds to the denoising residual, thereby yielding a clear objective function [20] that can be exploited in first-order optimization. Powerful denoisers such as denoising convolutional neural network (DnCNN) [66] typically do not meet the conditions of RED [45]. To address this limitation, Reehorst and Schniter introduced the score-matching by denoising (SMD) perspective to interpret RED [45]. Based on the fixed-point projection, Cohen et al. proposed the RED-PRO model [20] as a bridge between RED and PnP, while the hybrid steepest descent (HSD) method [63, 64] was employed to solve the resulting model. Meanwhile, Ryu et al. proved the convergence of PnP-FBS (forward-backward splitting) and PnP-ADMM using the Banach contraction principle under the assumption that the data term f is strongly convex and that the residual is nonexpansive [49]. However, enforcing strong convexity on f precludes many IR tasks [33]. Furthermore, Cohen et al. parameterized denoisers via the gradients of smooth potential functions that satisfy a symmetric Jacobian property [19], and Hurault, Leclaire, and Papadakis developed the gradient step (GS) denoiser [32, 33], which can be interpreted as a proximal operator of an implicit regularizer [33]. Although the convergence of PnP-ADMM is commonly analyzed from the perspective of Douglas-Rachford splitting (DRS) based on the equivalence between ADMM and DRS [49, 33], theoretically achieving fast fixed-point residual decay in PnP-DRS remains unknown.

Based on HPPP and PnP priors, we propose the gradient regularization by denoising via HPPP called GraRED-HP³ (Algorithm 3.2)¹. Our main contributions are as follows:

1. **Theoretical contributions.** The sequence $\{\mathbf{u}^k\}_{k \in \mathbb{N}}$ generated by HPPP with the positive semidefinite preconditioner \mathcal{M} converges strongly to a unique solution $\mathbf{u}^* = \arg \min_{\mathbf{u} \in \text{Fix}(\mathcal{T})} \|\mathbf{u} - \mathbf{a}\|_{\mathcal{M}}^2$, as stated in Theorem 3.1 and Proposition 3.2, while the original PPP method can only converge weakly to some uncertain solution. Moreover, compared with the asymptotic regularity result of PPP [9, Lemma 2.8] (i.e., $\lim_{k \rightarrow \infty} \|\mathcal{T} \mathbf{u}^k - \mathbf{u}^k\|_{\mathcal{M}} = 0$), we establish a convergence rate of $\mathcal{O}(1/k)$ for both $\|\mathcal{T} \mathbf{u}^k - \mathbf{u}^k\|$ and $\|\mathcal{T} \mathbf{u}^k - \mathbf{u}^k\|_{\mathcal{M}}$ (see Propositions 3.4 and 3.5).

¹Since the RED gradient exactly equals the residual, we adopt the GraRED notation—derived from Moreau decomposition—to represent the proximal operator of the implicit regularizer associated with the residual.

2. **Algorithmic development.** We integrate HPPP with denoiser priors to propose the GraRED-HP³ algorithm for IR problems and shed new theoretical insights on denoiser priors from a PPP standpoint. Noting that the PnP-ADMM algorithm can be reformulated in an equivalent DRS form [49, 33], and given that the worst-case convergence rate for DRS is $\mathcal{O}(1/\sqrt{k})$ [28], GraRED-HP³ improved a sublinear convergence rate (as per Proposition 3.5) and thereby serves as an accelerated PnP method.
3. **Experimental validation.** We numerically validate the advantages of HPPP, including its implicit regularity, acceleration, and efficiency, with several toy examples. In addition, we demonstrate the state-of-the-art performance of GraRED-HP³ and its restarted variant with advanced denoisers in IR tasks.

The rest of this paper is organized as follows. In section 2, we review some preliminaries for convergence analysis. In section 3, we analyze the convergence of HPPP. Combining HPPP and denoiser priors, we propose GraRED-HP³ for IR problems. In section 4, we verify the advantages of HPPP with several toy examples. Furthermore, we validate the performance of GraRED-HP³ through IR experiments. Finally, conclusions are presented in section 5.

2. Preliminaries. In this section, we provide some fundamental concepts related to the degenerate PPP method and denoiser priors. Let \mathcal{H} be a real Hilbert space with inner product $\langle \cdot, \cdot \rangle$ and corresponding induced norm $\|\cdot\|$, and let $\mathcal{A} : \mathcal{H} \rightarrow 2^{\mathcal{H}}$ be a (maybe multivalued) operator (that through the rest of this paper we often identify with its graph in $\mathcal{H} \times \mathcal{H}$).

2.1. Preconditioned proximal point. Bredies et al. [9] introduced the degenerate PPP framework with the positive semidefinite preconditioner $\mathcal{M} : \mathcal{H} \rightarrow \mathcal{H}$. The proper preconditioner \mathcal{M} can make $\mathcal{A} + \mathcal{M}$ have a lower triangular structure, which conveniently calculates the inverse $(\mathcal{A} + \mathcal{M})^{-1}$.

Definition 2.1. *An admissible preconditioner for the operator $\mathcal{A} : \mathcal{H} \rightarrow 2^{\mathcal{H}}$ is a bounded, linear, self-adjoint, and positive semidefinite operator $\mathcal{M} : \mathcal{H} \rightarrow \mathcal{H}$ such that*

$$\mathcal{T} = (\mathcal{M} + \mathcal{A})^{-1}\mathcal{M}$$

is single-valued and has full domain.

Therefore, the PPP iteration is written as

$$(2.1) \quad \mathbf{u}^0 \in \mathcal{H}, \mathbf{u}^{k+1} = \mathcal{T}\mathbf{u}^k = (\mathcal{M} + \mathcal{A})^{-1}\mathcal{M}\mathbf{u}^k.$$

If $\mathcal{M} = I$, then \mathcal{T} is a firmly nonexpansive (FNE) operator [2, Proposition 23.8] and (2.1) becomes the standard proximal point iteration. If \mathcal{M} is positive semidefinite, the operator \mathcal{T} is related with the degenerate \mathcal{M} -firmly nonexpansive (\mathcal{M} -FNE) operator [11, 15, 62, 9], which is associated with seminorm $\|\mathbf{u}\|_{\mathcal{M}} = \sqrt{\langle \mathcal{M}\mathbf{u}, \mathbf{u} \rangle}$ and semi inner-product $\langle \mathbf{u}, \mathbf{v} \rangle_{\mathcal{M}} = \langle \mathcal{M}\mathbf{u}, \mathbf{v} \rangle$. The following notion extends monotone characteristics, i.e., \mathcal{M} -monotonicity.

Definition 2.2 (\mathcal{M} -monotonicity). *Let $\mathcal{M} : \mathcal{H} \rightarrow \mathcal{H}$ be a bounded linear positive semidefinite operator; then $\mathcal{B} : \mathcal{H} \rightarrow 2^{\mathcal{H}}$ is \mathcal{M} -monotone if we have*

$$\langle \mathbf{v} - \mathbf{v}', \mathbf{u} - \mathbf{u}' \rangle_{\mathcal{M}} \geq 0 \quad \forall (\mathbf{u}, \mathbf{v}), (\mathbf{u}', \mathbf{v}') \in \mathcal{B}.$$

The following lemma demonstrates that the firmly nonexpansive notation can be generalized to the degenerate case [11, 15]. If \mathcal{M} is an admissible preconditioner and $\mathcal{M}^{-1}\mathcal{A}$ is \mathcal{M} -monotone, then the operator \mathcal{T} is \mathcal{M} -FNE.

Lemma 2.3 ([9]). *Let $\mathcal{A} : \mathcal{H} \rightarrow 2^{\mathcal{H}}$ be an operator with $\text{zer}\mathcal{A} \neq \emptyset$, and let \mathcal{M} be an admissible preconditioner such that $\mathcal{M}^{-1}\mathcal{A}$ is \mathcal{M} -monotone. Then \mathcal{T} is \mathcal{M} -FNE, i.e.,*

$$(2.2) \quad \|\mathcal{T}\mathbf{u} - \mathcal{T}\mathbf{v}\|_{\mathcal{M}}^2 + \|(I - \mathcal{T})\mathbf{u} - (I - \mathcal{T})\mathbf{v}\|_{\mathcal{M}}^2 \leq \|\mathbf{u} - \mathbf{v}\|_{\mathcal{M}}^2.$$

By the KM iteration, the degenerate PPP method is written as

$$(2.3) \quad \mathbf{u}^{k+1} = (1 - \lambda_k)\mathbf{u}^k + \lambda_k\mathcal{T}\mathbf{u}^k,$$

where λ_k is a sequence in $[0, 2]$ such that $\sum_{k \in \mathbb{N}} \lambda_k(2 - \lambda_k) = +\infty$.

2.2. PnP prior and RED.

2.2.1. PnP prior. Venkatakrishnan, Bouman, and Wohlberg proposed the first PnP method based on ADMM [56]. PnP methods replace the proximal mapping of the implicit regularizer defined by (2.4) with a denoiser $D_\sigma : \mathbb{R}^n \rightarrow \mathbb{R}^n$. PnP-ADMM (Algorithm 2.1) is well known for its fast empirical convergence and efficiency in computational imaging [35, 60]. Sreehari et al. established theoretical conditions for PnP-ADMM, requiring that the Jacobian ∇D_σ be a doubly stochastic and symmetric matrix with all real eigenvalues in the range $(0, 1]$ [51]. When the denoiser meets the necessary and sufficient conditions of Proposition 2.5, it is a proximal mapping of the implicit regularizer $\phi : \mathbb{R}^n \rightarrow \mathbb{R} \cup \{+\infty\}$. Subsequently, a nonlocal means denoiser satisfying these conditions was constructed [51].

Algorithm 2.1 PnP-ADMM

- 1: **Input:** Given $\mathbf{u}^0 = \mathbf{0}, \mathbf{x}^0, \mathbf{z}^0$ and total iterations $N > 0$
 - 2: **for** $k = 0, 1, 2, \dots, N - 1$ **do**
 - 3: $\mathbf{x}^{k+1} = D_\sigma(\mathbf{z}^k - \mathbf{u}^k)$
 - 4: $\mathbf{z}^{k+1} = \text{prox}_{\lambda f}(\mathbf{x}^{k+1} + \mathbf{u}^k)$
 - 5: $\mathbf{u}^{k+1} = \mathbf{u}^k + (\mathbf{x}^{k+1} - \mathbf{z}^{k+1})$
 - 6: **end for**
 - 7: **Output:** \mathbf{x}^N
-

Definition 2.4 ([5]). *The proximal operator of $\phi : \mathbb{R}^n \rightarrow \mathbb{R} \cup \{+\infty\}$ is defined by*

$$(2.4) \quad \text{prox}_\phi(\mathbf{x}) = \arg \min_{\mathbf{u} \in \mathbb{R}^n} \left\{ \frac{1}{2} \|\mathbf{u} - \mathbf{x}\|^2 + \phi(\mathbf{u}) \right\}.$$

Proposition 2.5 ([40, 25]). *A function $h : \mathbb{R}^n \rightarrow \mathbb{R}^n$ defined everywhere is the proximal operator of a proper convex lower semicontinuous function $\phi : \mathbb{R}^n \rightarrow \mathbb{R} \cup \{+\infty\}$ if and only if the following conditions hold jointly:*

- (a) *There exists a convex lower semicontinuous function ψ such that for each $\mathbf{x} \in \mathbb{R}^n$, $h(\mathbf{x}) = \nabla\psi(\mathbf{x})$;*
- (b) *h is nonexpansive, i.e.,*

$$\|h(\mathbf{x}) - h(\mathbf{y})\| \leq \|\mathbf{x} - \mathbf{y}\| \quad \forall \mathbf{x}, \mathbf{y} \in \mathbb{R}^n.$$

2.2.2. RED prior. RED [47] is defined by

$$(2.5) \quad g_{\text{red}}(\mathbf{x}) = \frac{1}{2} \langle \mathbf{x}, \mathbf{x} - D_{\sigma}(\mathbf{x}) \rangle,$$

where $D_{\sigma} : \mathbb{R}^n \rightarrow \mathbb{R}^n$ is a denoiser which is assumed to obey the following assumptions:

(C1) Local homogeneity: For all $\mathbf{x} \in \mathbb{R}^n$, $D_{\sigma}((1 + \epsilon)x) = (1 + \epsilon)D_{\sigma}(\mathbf{x})$ for sufficiently small $\epsilon > 0$.

(C2) Differentiability: The denoiser $D_{\sigma}(\cdot)$ is differentiable.

(C3) Jacobian symmetry [45]: $[\nabla D_{\sigma}(\mathbf{x})]^T = \nabla D_{\sigma}(\mathbf{x})$ for all $\mathbf{x} \in \mathbb{R}^n$.

(C4) Strong passivity: The spectral radius of the Jacobian satisfies $\eta(\nabla D_{\sigma}(\mathbf{x})) \leq 1$.

If $D_{\sigma}(\mathbf{x})$ satisfies **C1**, **C2**, and **C3**, then $\nabla g_{\text{red}}(\mathbf{x}) = \mathbf{x} - D_{\sigma}(\mathbf{x}) = R(\mathbf{x})$. Moreover, if the denoiser satisfies **C4**, then RED is convex and D_{σ} is nonexpansive.

2.2.3. Implicit Gradient RED. The gradient of RED is exactly the denoising residual. We show that under ideal conditions and assuming the residual is nonexpansive, both the denoiser and its residual function are proximal operators of implicit regularizers. Even if all RED conditions are hard to satisfy, learning FNE operators can still achieve this.

The nonexpansive assumption has theoretically played a crucial role in PnP prior and RED. Ryu et al. proposed the following assumption to guarantee the convergence of PnP methods [49]:

$$(A) \quad \|(I - D_{\sigma})(\mathbf{u}) - (I - D_{\sigma})(\mathbf{v})\| \leq \varepsilon \|\mathbf{u} - \mathbf{v}\|;$$

for any $\mathbf{u}, \mathbf{v} \in \mathbb{R}^n$ and $\varepsilon \leq 1$, the real spectral normalization is used to obtain nonexpansive residual. Under the conditions **C1**, **C2**, **C3**, and **C4** of RED and assumption (A), we can further discuss the relationship between ∇g_{red} and the proximal operator, and we prove that there exists an implicit regularizer ϕ such that $D_{\sigma}(\mathbf{x}) = \text{prox}_{\phi}(\mathbf{x})$ and $R(\mathbf{x}) = \nabla g_{\text{red}}(\mathbf{x}) = \text{prox}_{\phi^*}(\mathbf{x})$, where ϕ^* is the conjugate of ϕ .

Lemma 2.6. *Assume that a denoiser $D_{\sigma} : \mathbb{R}^n \rightarrow \mathbb{R}^n$ satisfies conditions **C1**, **C2**, **C3**, **C4** and assumption (A); then there exists an implicit regularizer $\phi : \mathbb{R}^n \rightarrow \mathbb{R} \cup \{+\infty\}$ such that*

$$(2.6) \quad D_{\sigma}(\mathbf{x}) = \text{prox}_{\phi}(\mathbf{x}), R(\mathbf{x}) = \text{prox}_{\phi^*}(\mathbf{x}).$$

Proof. By assumption conditions, the RED term g_{red} is convex, and $\nabla g_{\text{red}} = I - D_{\sigma} = R$. Let $\psi(\mathbf{x}) = \frac{1}{2} \|\mathbf{x}\|^2 - g_{\text{red}}$, then $D_{\sigma} = I - \nabla g_{\text{red}} = \nabla \psi$, which is a GS denoiser. Since R is nonexpansive and D_{σ} is differentiable, then $\eta(\nabla^2 \psi) = \eta(\nabla D_{\sigma}) = \eta(I - \nabla R) \in [0, 1]$, it follows that ψ is convex. Applying Proposition 2.5, together with $h(\mathbf{x}) = D_{\sigma}(\mathbf{x})$, $\psi = \frac{1}{2} \|\mathbf{x}\|^2 - g_{\text{red}}$ and Moreau decomposition [5, Theorem 6.44], i.e., $\text{prox}_{\phi}(\mathbf{x}) + \text{prox}_{\phi^*}(\mathbf{x}) = \mathbf{x}$, there exists a function ϕ and its conjugate ϕ^* such that $D_{\sigma}(\mathbf{x}) = \nabla \psi(\mathbf{x}) = \text{prox}_{\phi}(\mathbf{x})$, and $R(\mathbf{x}) = \text{prox}_{\phi^*}(\mathbf{x})$, which completes the proof. ■

Satisfying all RED conditions is challenging; in practice, only the nonexpansiveness assumption is required. From the perspective of monotone operator theory, Lemma 2.7 [2, Corollary 23.9] provides a necessary and sufficient condition for a denoiser to be a proximal operator of an implicit regularizer.

Lemma 2.7. *The mapping $T : \mathcal{X} \rightarrow \mathcal{X}$ is the resolvent of a maximal monotone operator if and only if T is FNE.*

Moreover, by [2, Proposition 4.4], the operator T is FNE if and only if there exists a nonexpansive operator $S : \mathcal{X} \rightarrow \mathcal{X}$ such that $T = \frac{S+I}{2}$. Therefore, the core issue in explaining denoiser prior as a proximal operator of a convex regularizer is training a nonexpansive operator. Recent developments, such as spectral normalization [49, 21], learning maximally monotone operators [42], learning FNE denoisers [54, 10], and learning pseudocontractive denoisers [57], have made the nonexpansive assumption more realistic in practice. Constructing the FNE denoiser D_σ is feasible, similarly, the residual $R = I - D_\sigma$ can be FNE in (2.2) with $\mathcal{M} = I$. Both can be proximal operators of implicit regularizers.

3. Halpern-type preconditioned proximal point (HPPP). Compared with KM iteration, the classic Halpern iteration offers the advantage of strong convergence in infinite-dimensional Hilbert spaces [29]. The Halpern iteration $\mathbf{u}^{k+1} = \lambda_{k+1}\mathbf{u}^0 + (1 - \lambda_{k+1})T\mathbf{u}^k$ [26] is an implicitly regularized method for finding a particular fixed point [22], and the sequence $\{\mathbf{u}^k\}_{k \in \mathbb{N}}$ generated by the Halpern iteration with suitable $\{\lambda_k\}_{k \in \mathbb{N}}$ strongly converges to the projection $P_{\text{Fix}(T)}(\mathbf{u}^0)$ [26, 37, 58, 30, 61, 44, 29], where $P_{\text{Fix}(T)}(\mathbf{u}^0) = \arg \min_{\mathbf{u} \in \text{Fix}(T)} \|\mathbf{u} - \mathbf{u}^0\|^2$. When PPP is used to solve the inclusion problem (1.3), the sequence $\{\mathbf{u}^k\}_{k \in \mathbb{N}}$ generated by PPP can only converge weakly to some uncertain fixed point of \mathcal{T} . Based on the Halpern iteration, we propose the Halpern-type preconditioned proximal point (HPPP) algorithms (1.5).

3.1. Convergence analysis. First, we analyze the convergence of the sequence $\{\mathbf{u}^k\}_{k \in \mathbb{N}}$ generated by HPPP (1.5). If \mathcal{T} satisfies the mild condition $\|\mathcal{T}\mathbf{u} - \mathcal{T}\mathbf{v}\| \leq C\|\mathbf{u} - \mathbf{v}\|_{\mathcal{M}}$ ($C > 0$) [9], then there exists a unique solution $\mathbf{u}^* = \arg \min_{\mathbf{u} \in \text{Fix}(\mathcal{T})} \|\mathbf{u} - \mathbf{a}\|_{\mathcal{M}}^2$, which corresponds to the \mathcal{M} -projection of \mathbf{a} onto $\text{Fix}(\mathcal{T})$ from Lemma B.3. In the subsequent analysis, the notation \mathbf{u}^* will always denote this \mathcal{M} -projection. We use " \rightarrow " for *strong convergence* and " \rightharpoonup " for *weak convergence*.

Theorem 3.1. *Let $\mathcal{A} : \mathcal{H} \rightarrow 2^{\mathcal{H}}$ be an operator with $\text{zer}\mathcal{A} \neq \emptyset$, and let \mathcal{M} be an admissible preconditioner such that $\mathcal{M}^{-1}\mathcal{A}$ is \mathcal{M} -monotone and $(\mathcal{M} + \mathcal{A})^{-1}$ is L -Lipschitz. Let $\{\mathbf{u}^k\}$ be the sequence generated by HPPP (1.5). Assume that every weak cluster point of $\{\mathbf{u}^k\}_{k \in \mathbb{N}}$ lies in $\text{Fix}(\mathcal{T})$, and that $\{\mu_k\}_{k \in \mathbb{N}}$ satisfies*

- (i) $\lim_{k \rightarrow \infty} \mu_k = 0$,
- (ii) $\sum_{k \in \mathbb{N}} \mu_k = +\infty$,
- (iii) $\lim_{k \rightarrow \infty} \frac{\mu_{k+1} - \mu_k}{\mu_k} = 0$ or $\sum_{k \in \mathbb{N}} |\mu_{k+1} - \mu_k| < \infty$.

Then $\{\mathbf{u}^k\}_{k \in \mathbb{N}}$ converges strongly to \mathbf{u}^ .*

Proof. First, we show $\lim_{k \rightarrow \infty} \|\mathbf{u}^k - \mathbf{u}^*\|_{\mathcal{M}} = 0$. Based on the definition of the upper limit, we take a subsequence $\{\mathbf{u}^{k_n}\}_{n \in \mathbb{N}}$ of $\{\mathbf{u}^k\}_{k \in \mathbb{N}}$ such that

$$(3.1) \quad \limsup_{k \rightarrow \infty} \left\langle \mathbf{a} - \mathbf{u}^*, \mathcal{T}\mathbf{u}^k - \mathbf{u}^* \right\rangle_{\mathcal{M}} = \lim_{n \rightarrow \infty} \left\langle \mathbf{a} - \mathbf{u}^*, \mathcal{T}\mathbf{u}^{k_n} - \mathbf{u}^* \right\rangle_{\mathcal{M}}.$$

By Lemma A.2(i), the sequence $\{\mathbf{u}^{k_n}\}_{n \in \mathbb{N}}$ is bounded, there exists a weakly convergent subsequence $\{\mathbf{u}^{k_{n_j}}\}_{j \in \mathbb{N}}$, and we may assume $\mathbf{u}^{k_{n_j}} \rightharpoonup \tilde{\mathbf{u}}$. According to the conditions of the theorem, we have $\tilde{\mathbf{u}} \in \text{Fix}(\mathcal{T})$.

Applying Lemma A.2, together with conditions (i)-(iii), we obtain $\mathcal{T}\mathbf{u}^k - \mathbf{u}^k \rightarrow \mathbf{0}$; then $\langle \mathbf{a} - \mathbf{u}^*, \mathcal{T}\mathbf{u}^k - \mathbf{u}^k \rangle_{\mathcal{M}} \rightarrow 0$. Hence, we have

$$\begin{aligned} \lim_{n \rightarrow \infty} \langle \mathbf{a} - \mathbf{u}^*, \mathcal{T}\mathbf{u}^{k_{n_j}} - \mathbf{u}^* \rangle_{\mathcal{M}} &= \lim_{j \rightarrow \infty} \langle \mathbf{a} - \mathbf{u}^*, (\mathcal{T}\mathbf{u}^{k_{n_j}} - \mathbf{u}^{k_{n_j}}) + (\mathbf{u}^{k_{n_j}} - \mathbf{u}^*) \rangle_{\mathcal{M}} \\ &= \lim_{j \rightarrow \infty} \langle \mathbf{a} - \mathbf{u}^*, \mathbf{u}^{k_{n_j}} - \mathbf{u}^* \rangle_{\mathcal{M}} \\ &= \langle \mathbf{a} - \mathbf{u}^*, \tilde{\mathbf{u}} - \mathbf{u}^* \rangle_{\mathcal{M}}. \end{aligned}$$

By Lemma B.1, we have

$$(3.2) \quad \limsup_{k \rightarrow \infty} \langle \mathbf{a} - \mathbf{u}^*, \mathcal{T}\mathbf{u}^k - \mathbf{u}^* \rangle_{\mathcal{M}} = \langle \mathbf{a} - \mathbf{u}^*, \tilde{\mathbf{u}} - \mathbf{u}^* \rangle_{\mathcal{M}} \leq 0.$$

Denoting $\delta_{k+1} = \mu_{k+1} \|\mathbf{a} - \mathbf{u}^*\|_{\mathcal{M}}^2 + 2(1 - \mu_{k+1}) \langle \mathbf{a} - \mathbf{u}^*, \mathcal{T}\mathbf{u}^k - \mathbf{u}^* \rangle_{\mathcal{M}}$, noticing that

$$\begin{aligned} \|\mathbf{u}^{k+1} - \mathbf{u}^*\|_{\mathcal{M}}^2 &= \left\| \mu_{k+1}(\mathbf{a} - \mathbf{u}^*) + (1 - \mu_{k+1})(\mathcal{T}\mathbf{u}^k - \mathbf{u}^*) \right\|_{\mathcal{M}}^2 \\ &= \mu_{k+1}^2 \|\mathbf{a} - \mathbf{u}^*\|_{\mathcal{M}}^2 + (1 - \mu_{k+1})^2 \|\mathcal{T}\mathbf{u}^k - \mathbf{u}^*\|_{\mathcal{M}}^2 \\ &\quad + 2\mu_{k+1}(1 - \mu_{k+1}) \langle \mathbf{a} - \mathbf{u}^*, \mathcal{T}\mathbf{u}^k - \mathbf{u}^* \rangle_{\mathcal{M}} \\ &\leq (1 - \mu_{k+1}) \|\mathbf{u}^k - \mathbf{u}^*\|_{\mathcal{M}}^2 + \mu_{k+1} \delta_{k+1}, \end{aligned}$$

and applying Lemma A.1, together with conditions (i)-(ii) and $\limsup_{k \rightarrow \infty} \delta_k \leq 0$, we have $\lim_{k \rightarrow \infty} \|\mathbf{u}^k - \mathbf{u}^*\|_{\mathcal{M}} = 0$.

By the definition of \mathbf{u}^{k+1} we immediately obtain

$$(3.3) \quad \begin{aligned} \|\mathbf{u}^{k+1} - \mathbf{u}^*\| &= \left\| \mu_{k+1}(\mathbf{a} - \mathbf{u}^*) + (1 - \mu_{k+1})(\mathcal{T}\mathbf{u}^k - \mathbf{u}^*) \right\| \\ &\leq \mu_{k+1} \|\mathbf{a} - \mathbf{u}^*\| + (1 - \mu_{k+1}) \|\mathcal{T}\mathbf{u}^k - \mathbf{u}^*\| \\ &\leq \mu_{k+1} \|\mathbf{a} - \mathbf{u}^*\| + C(1 - \mu_{k+1}) \|\mathbf{u}^k - \mathbf{u}^*\|_{\mathcal{M}}, \end{aligned}$$

where the last inequality follows from (A.3) and C is defined as in (A.2). Since $\lim_{k \rightarrow \infty} \mu_k = 0$ and $\lim_{k \rightarrow \infty} \|\mathbf{u}^k - \mathbf{u}^*\|_{\mathcal{M}} = 0$, combined with (3.3) they yield that

$$\lim_{k \rightarrow \infty} \|\mathbf{u}^k - \mathbf{u}^*\| = 0,$$

which ends the proof of Theorem 3.1. ■

It is easy to verify that $\mu_k = \frac{1}{k^\alpha}$ ($0 < \alpha \leq 1$) satisfies conditions (i)-(iii) of Theorem 3.1. Compared with [3], we have provided an alternative method to obtain the limit point as the \mathcal{M} -projection of the initial point. The work [3] requires that \mathcal{A} be linear, whereas we consider a more general case for \mathcal{A} . By introducing the maximal monotonicity assumption on \mathcal{A} , we can prove that every weak cluster point \mathbf{u} of $\{\mathbf{u}^k\}_{k \in \mathbb{N}}$ lies in $\text{Fix}(\mathcal{T})$. According to Theorem 3.1, we obtain the following proposition.

Proposition 3.2. *If the conditions of Theorem 3.1 hold, and $\mathcal{A} : \mathcal{H} \rightarrow 2^{\mathcal{H}}$ is a maximal monotone operator, then $\{\mathbf{u}^k\}_{k \in \mathbb{N}}$ converges strongly to \mathbf{u}^* .*

Proof. Assume that $\mathbf{u}^{k_n} \rightharpoonup \mathbf{u}$. By Lemma A.2(iii), we have $\mathcal{T}\mathbf{u}^{k_n} - \mathbf{u}^{k_n} \rightarrow \mathbf{0}$, and it follows that

$$\mathcal{T}\mathbf{u}^{k_n} = (\mathcal{T}\mathbf{u}^{k_n} - \mathbf{u}^{k_n}) + \mathbf{u}^{k_n} \rightarrow \mathbf{0} + \mathbf{u} = \mathbf{u},$$

i.e., $\mathcal{T}\mathbf{u}^{k_n} \rightarrow \mathbf{u}$. Using $\mathcal{T}\mathbf{u}^{k_n} - \mathbf{u}^{k_n} \rightarrow \mathbf{0}$, we have

$$\mathcal{A}\mathcal{T}\mathbf{u}^{k_n} \ni \mathcal{M}(\mathbf{u}^{k_n} - \mathcal{T}\mathbf{u}^{k_n}) \rightarrow \mathbf{0}.$$

Since \mathcal{A} is maximal, we have that \mathcal{A} is closed in $\mathcal{H}_{weak} \times \mathcal{H}_{strong}$ [2, Proposition 20.38], and hence $\mathbf{0} \in \mathcal{A}\mathbf{u}$, i.e., $\mathbf{u} \in \text{zer}\mathcal{A} = \text{Fix}(\mathcal{T})$. Thus, we prove that every weak cluster point of $\{\mathbf{u}^k\}_{k \in \mathbb{N}}$ lies in $\text{Fix}(\mathcal{T})$. This completes the proof of Proposition 3.2. \blacksquare

Remark 1. *We compare Theorem 3.1, Proposition 3.2 with [9, Theorem 2.9] and [9, Corollary 2.10], where the sequence $\{\mathbf{u}^k\}_{k \in \mathbb{N}}$ generated by HPPP converges strongly to a particular fixed point of \mathcal{T} . All conditions are the same, except for the additional assumption about $\{\mu_k\}_{k \in \mathbb{N}}$. The Lipschitz regularity of $(\mathcal{M} + \mathcal{A})^{-1}$ is a mild assumption, especially in applications to splitting algorithms, and is used to prove the uniqueness of \mathcal{M} -projection and guarantee the boundedness of $\{\mathbf{u}^k\}_{k \in \mathbb{N}}, \{\mathcal{T}\mathbf{u}^k\}_{k \in \mathbb{N}}$.*

Hundal constructed an example in which the alternating projection $(P_U P_V)^k \mathbf{x}^0$ converges weakly but not strongly [31], where U is a closed convex cone and V is a closed hyperplane. Building on Hundal's counterexample, [13] showed that the weak convergence of the DRS algorithm cannot be improved to strong convergence. Similarly, using the same counterexample, we can demonstrate that PPP also fails to converge strongly.

Counterexample 1. *Suppose that \mathcal{H} is infinite-dimensional and separable. Let V and U be Hundal's hyperplane and Hundal's cone, respectively, and set*

$$\mathcal{A}_1 : \mathbf{x} \mapsto \begin{cases} V^\perp & \text{if } \mathbf{x} \in V, \\ \emptyset & \text{if } \mathbf{x} \notin V, \end{cases} \quad \text{and } \mathcal{A}_2 = (P_V \circ P_U \circ P_V)^{-1} - I.$$

Then the sequence $\{\mathbf{u}^k\}_{k \in \mathbb{N}}$ generated by PPP (2.3) with $\lambda_k = 1$ converges weakly, but not strongly, to a zero of $\mathcal{A}_1 + \mathcal{A}_2$.

Proof. As proved in [13], the operators \mathcal{A}_1 and \mathcal{A}_2 are maximally monotone, and $\mathbf{0} \in \text{zer}(\mathcal{A}_1 + \mathcal{A}_2)$, and the sequence $\{\mathbf{w}^k\}_{k \in \mathbb{N}}$

$$(3.4) \quad \mathbf{w}^{k+1} = \mathbf{w}^k + J_{\mathcal{A}_2}(2J_{\mathcal{A}_1}\mathbf{w}^k - \mathbf{w}^k) - J_{\mathcal{A}_1}\mathbf{w}^k,$$

generated by the DRS algorithm can weakly converge to $\mathbf{0}$ and $\mathbf{w}^k \not\rightarrow \mathbf{0}$.

The sequence (3.4) can be viewed as a special PPP with

$$\mathcal{A} = \begin{pmatrix} \mathcal{A}_1 & I \\ -I & \mathcal{A}_2 \end{pmatrix}, \quad \mathcal{M} = \begin{pmatrix} I & -I \\ -I & I \end{pmatrix},$$

and $\mathbf{w}^k = \mathcal{C}^* \mathbf{u}^k = \mathbf{x}^k - \mathbf{y}^k$, where $\mathcal{C}^* = (I, -I)$. By [9, Corollary 2.15], $\mathbf{u}^k \rightharpoonup \mathbf{0}$. Indeed, if by contraction, $\mathbf{u}^k \rightarrow \mathbf{0}$, then

$$\|\mathbf{w}^k - \mathbf{0}\| = \|\mathcal{C}^* \mathbf{u}^k - \mathbf{0}\| \leq \|\mathcal{C}\| \cdot \|\mathbf{u}^k - \mathbf{0}\| \rightarrow 0,$$

which contradicts the fact that $\mathbf{w}^k \not\rightarrow \mathbf{0}$. Thus $\{\mathbf{u}^k\}_{k \in \mathbb{N}}$ can only converge weakly to $\mathbf{0}$. \blacksquare

Remark 2. From Counterexample 1, HPPP has a strong convergence advantage over PPP in infinite-dimensional spaces, which has important theoretical value.

Remark 3. Regarding the choice of the anchor point, we can use the degraded observed image, the denoised image, or the restarted technique (see Algorithm 3.1). The restarted technique is an effective method in machine learning [41] and LP [17, 38].

Algorithm 3.1 Restarted HPPP

Input: Initialization $\mathbf{u}^{0,0} = \mathbf{a}^0$, total iteration $N > 0$, period $q > 0$, and epoch $N_e = \lfloor \frac{N}{q} \rfloor$

- 1: **for** $n = 1, 2, \dots, N_e$ **do**
- 2: **for** $k = 0, 1, \dots, q - 1$ **do**
- 3: $\mathbf{u}^{n,k+1} = \text{HPPP}(\mathbf{u}^{n,k}, \mathbf{a}^n)$
- 4: **end for**
- 5: $\mathbf{a}^{n+1} = \mathbf{u}^{n,q}$
- 6: **end for**

Output: $\mathbf{u}^{N_e,q}$

3.2. Convergence rate. Based on the following technical lemma, Sabach and Shtern [50] first showed that, for a general form of Halpern iteration, the fixed-point residual converges at a rate of $\mathcal{O}(1/k)$.

Lemma 3.3 ([50]). Let $M_1 > 0$. Assume that $\{a_k\}_{k \in \mathbb{N}}$ is a sequence of nonnegative real numbers such that $a_1 < M_1$ and

$$a_{k+1} \leq (1 - \gamma b_{k+1})a_k + (b_k - b_{k+1})c_k, k \geq 1,$$

where $\gamma \in (0, 1]$, the sequence $\{b_k\}_{k \in \mathbb{N}}$ is defined as in $b_k = \min\{\frac{2}{\gamma k}, 1\}$, and $\{c_k\}_{k \in \mathbb{N}}$ is a sequence of real numbers such that $c_k \leq M_1 < \infty$. Then the sequence $\{a_k\}_{k \in \mathbb{N}}$ satisfies

$$a_k \leq \frac{M_1 J}{\gamma k}, k \geq 1,$$

where $J = \lfloor \frac{2}{\gamma} \rfloor$.

By applying Lemma 3.3, we will establish a sublinear convergence rate for $\|\mathbf{u}^k - \mathbf{u}^{k-1}\|$ and fixed-point residual $\|\mathcal{T}\mathbf{u}^k - \mathbf{u}^k\|$ or $\|\mathcal{T}\mathbf{u}^k - \mathbf{u}^k\|_{\mathcal{M}}$.

Proposition 3.4. Let $\mathcal{A} : \mathcal{H} \rightarrow 2^{\mathcal{H}}$ be a maximal operator with $\text{zer}\mathcal{A} \neq \emptyset$, and let \mathcal{M} be an admissible preconditioner such that $\mathcal{M}^{-1}\mathcal{A}$ is \mathcal{M} -monotone and $(\mathcal{M} + \mathcal{A})^{-1}$ is L -Lipschitz. Let $\{u^k\}$ be the sequence generated by (1.5). If $\mu_k = \min\{\frac{2}{k}, 1\}$, then

- (i) $\|\mathbf{u}^k - \mathbf{u}^{k-1}\|_{\mathcal{M}} \leq \frac{2M}{k}$, i.e., $\|\mathbf{u}^k - \mathbf{u}^{k-1}\|_{\mathcal{M}} = \mathcal{O}\left(\frac{1}{k}\right)$;
(ii) $\|\mathbf{u}^{k+1} - \mathbf{u}^k\| = \mathcal{O}\left(\frac{1}{k}\right)$, $\|\mathbf{u}^k - \mathcal{T}\mathbf{u}^k\| = \mathcal{O}\left(\frac{1}{k}\right)$.

Proof. (i) According to (A.7), we have

$$\|\mathbf{u}^{k+1} - \mathbf{u}^k\|_{\mathcal{M}} \leq (1 - \mu_{k+1}) \|\mathbf{u}^k - \mathbf{u}^{k-1}\|_{\mathcal{M}} + M |\mu_{k+1} - \mu_k|,$$

where $M = \|\mathbf{a} - \mathbf{u}^*\|_{\mathcal{M}} + C_1$, $\mathbf{u}^* \in \text{Fix}(\mathcal{T})$, and C_1 is defined as in (A.4). Applying Lemma 3.3 together with $c_k = M_1 = M$, $J = 2$, $\gamma = 1$, $a_k = \|\mathbf{u}^k - \mathbf{u}^{k-1}\|_{\mathcal{M}}$, and $\mu_k = b_k$ to the above inequality, we have $\|\mathbf{u}^k - \mathbf{u}^{k-1}\|_{\mathcal{M}} \leq \frac{2M}{k}$.

(ii) By (A.10), when $k \geq 2$ we have

$$\begin{aligned} \|\mathbf{u}^{k+1} - \mathbf{u}^k\| &\leq C(1 - \mu_{k+1}) \|\mathbf{u}^k - \mathbf{u}^{k-1}\|_{\mathcal{M}} + M' |\mu_{k+1} - \mu_k| \\ &\leq \frac{2MC}{k} + \frac{2M'}{k(k+1)} = \mathcal{O}\left(\frac{1}{k}\right), \end{aligned}$$

where the second inequality follows from (i) and the fact that $\mu_k - \mu_{k+1} = \frac{2}{k(k+1)}$ ($k \geq 2$), and $M' = \|\mathbf{a} - \mathbf{u}^*\| + CC_1$, and C, C_1 are defined in (A.2) and (A.4), respectively.

As for the second result, by the triangle inequality and $\mathbf{u}^{k+1} - \mathcal{T}\mathbf{u}^k = \mu_{k+1}(\mathbf{a} - \mathcal{T}\mathbf{u}^k)$, for $k \geq 2$,

$$\begin{aligned} \|\mathbf{u}^k - \mathcal{T}\mathbf{u}^k\| &\leq \|\mathbf{u}^k - \mathbf{u}^{k+1}\| + \|\mathbf{u}^{k+1} - \mathcal{T}\mathbf{u}^k\| \\ &\leq \|\mathbf{u}^k - \mathbf{u}^{k+1}\| + \mu_{k+1} \|\mathbf{a} - \mathcal{T}\mathbf{u}^k\| \\ &\leq \frac{2MC}{k} + \frac{2M'}{k(k+1)} + \frac{2M'}{k+1} = \mathcal{O}\left(\frac{1}{k}\right). \quad \blacksquare \end{aligned}$$

Let $\mathcal{M} = \mathcal{C}\mathcal{C}^*$ be a decomposition of \mathcal{M} according to [9, Proposition 2.3]. By [9, Theorem 2.13], the operator $\tilde{\mathcal{T}} = \mathcal{C}^*(\mathcal{M} + \mathcal{A})^{-1}\mathcal{C}$ is FNE. Let $\mathbf{w}^k = \mathcal{C}^*\mathbf{u}^k$ and $\mathbf{a} = \mathbf{u}^0$, and then HPPP is equivalent to the following reduced algorithm:

$$(3.5) \quad \mathbf{w}^0 = \mathcal{C}^*\mathbf{u}^0, \mathbf{w}^{k+1} = \mu_{k+1}\mathbf{w}^0 + (1 - \mu_{k+1})\tilde{\mathcal{T}}\mathbf{w}^k.$$

By [36, Theorem 2.1] and [52, Proposition 2.9], we further give the following (tight) optimal convergence rate for HPPP.

Proposition 3.5. *Let $\mathcal{A} : \mathcal{H} \rightarrow 2^{\mathcal{H}}$ be a maximal operator with $\text{zer}\mathcal{A} \neq \emptyset$, and let \mathcal{M} be an admissible preconditioner such that $\mathcal{M}^{-1}\mathcal{A}$ is \mathcal{M} -monotone and $(\mathcal{M} + \mathcal{A})^{-1}$ is L -Lipschitz. Let $\{\mathbf{u}^k\}_{k \in \mathbb{N}}, \{\mathbf{w}^k\}_{k \in \mathbb{N}}$ be the sequences generated by (1.5) and (3.5). If $\mu_k = \frac{1}{k+1}$ and $\mathbf{a} = \mathbf{u}^0$, then*

- (i) $\|\mathbf{w}^k - \tilde{\mathcal{T}}\mathbf{w}^k\| \leq \frac{2\|\mathbf{w}^0 - \mathbf{w}^*\|}{k+1}$ for $k \geq 0$ and $\mathbf{w}^* \in \text{Fix}(\tilde{\mathcal{T}})$,
(ii) $\|\mathbf{u}^k - \mathcal{T}\mathbf{u}^k\|_{\mathcal{M}} \leq \frac{2\|\mathbf{u}^0 - \mathbf{u}^*\|_{\mathcal{M}}}{k+1}$ for $k \geq 0$ and $\mathbf{u}^* \in \text{Fix}(\mathcal{T})$.

3.3. GraRED-HP³. The primal-dual algorithm for solving (1.4) is viewed as the fixed-point iteration $\mathbf{u}^{k+1} = \mathcal{T}\mathbf{u}^k = (\mathcal{A} + \mathcal{M})^{-1}\mathcal{M}\mathbf{u}^k$ with $\mathcal{A} = \begin{pmatrix} \lambda\partial f & \mathbf{K}^* \\ -\mathbf{K} & \partial g^* \end{pmatrix}$, $\mathcal{M} = \begin{pmatrix} \frac{1}{\tau}I & -\mathbf{K}^* \\ -\mathbf{K} & \frac{1}{s}I \end{pmatrix}$. Under the degenerate case $\tau s \|\mathbf{K}\|^2 = 1$, the HPPP iteration is given by

$$(3.6) \quad \begin{cases} \mathbf{d}^k &= (I + \tau\lambda\partial f)^{-1}(\mathbf{x}^k - \tau\mathbf{K}^*\mathbf{y}^k), \\ \mathbf{x}^{k+1} &= \mu_{k+1}\mathbf{x}_a + (1 - \mu_{k+1})\mathbf{d}^k, \\ \mathbf{y}^{k+1} &= \mu_{k+1}\mathbf{y}_a + (1 - \mu_{k+1})(I + s\partial g^*)^{-1}(\mathbf{y}^k + s\mathbf{K}(2\mathbf{d}^k - \mathbf{x}^k)), \end{cases}$$

where $\mathbf{a} = (\mathbf{x}_a, \mathbf{y}_a)$, $(\mathbf{x}_0, \mathbf{y}_0) \in \mathcal{X} \times \mathcal{Y}$ are the anchor and initial points. Under the ideal conditions of RED and with assumption (A), according to Lemma 2.6, both the denoiser D_σ and the residual R can be expressed as the proximal operators of implicit regularizers, i.e., $D_\sigma(\mathbf{x}) = \text{prox}_\phi(\mathbf{x})$, $R(\mathbf{x}) = \text{prox}_{\phi^*}(\mathbf{x})$. Let $g(\mathbf{x}) = \frac{\phi(s\mathbf{x})}{s}$; then $\phi^* = sg^*$ [5, Theorem 4.14], and we can replace $(I + s\partial g^*)^{-1}$ with the residual R in (3.6). Set $\mathbf{K} = I$; the implicit gradient RED via HPPP called GraRED-HP³ is proposed in Algorithm 3.2. Even if the conditions of RED are difficult to meet [45], recent developments [49, 54, 42, 21, 15, 10, 57] can learn FNE denoisers. According to Lemma 2.7, both the denoiser and the residual still act as the proximal operators of implicit regularizers.

3.3.1. Acceleration for PnP methods. PnP-ADMM (see Algorithm 2.1) is a well-known method for solving (1.1), which can be written into an equivalent DRS form [49, 33], i.e., $\mathbf{w}^{k+1} = \tilde{\mathcal{T}}\mathbf{w}^k = \mathbf{w}^k + D_\sigma(2\text{prox}_{\lambda f}(\mathbf{w}^k) - \mathbf{w}^k) - \text{prox}_{\lambda f}(\mathbf{w}^k)$. When $\mathbf{w}^k = \mathbf{x}^k - \mathbf{y}^k$, $\tau = s = 1$, $\mu_k = 0$ in GraRED-HP³ results exactly in the DRS iteration. Thus, PnP-DRS is a special case of GraRED-HP³, which can be obtained from the perspective of PPP [11, 9]. The related GraRED-P³ algorithm is shown in Algorithm 3.3. Furthermore, Proposition 3.5 demonstrates that GraRED-HP³ is an accelerated PnP method achieving an $\mathcal{O}(1/k)$ convergence rate for the fixed-point residual.

Remark 4. In [28], a worst-case convergence rate of $\mathcal{O}\left(\frac{1}{\sqrt{k}}\right)$ for $\|\mathbf{w}^k - \tilde{\mathcal{T}}\mathbf{w}^k\|$ was established for DRS, which also applies to PnP-ADMM. In contrast, GraRED-HP³ obtains an accelerated convergence rate of $\mathcal{O}\left(\frac{1}{k}\right)$ for $\|\mathbf{w}^k - \tilde{\mathcal{T}}\mathbf{w}^k\|$.

Algorithm 3.2 GraRED-HP³

Input: Initialization $\mathbf{u}^0 = (\mathbf{x}^0, \mathbf{y}^0) \in \mathbb{R}^n \times \mathbb{R}^n$, anchor point $\mathbf{a} = (\mathbf{x}_a, \mathbf{y}_a) \in \mathbb{R}^n \times \mathbb{R}^n$, iteration number $N > 0$, and $R = I - D_\sigma$ is the residual.

- 1: **for** $k = 0, 1, 2, \dots, N - 1$ **do**
- 2: $\mathbf{d}^k = \text{prox}_{\lambda f}(\mathbf{x}^k - \tau\mathbf{y}^k)$
- 3: $\mathbf{x}^{k+1} = \mu_{k+1}\mathbf{x}_a + (1 - \mu_{k+1})\mathbf{d}^k$
- 4: $\mathbf{y}^{k+1} = \mu_{k+1}\mathbf{y}_a + (1 - \mu_{k+1})R(\mathbf{y}^k + s(2\mathbf{d}^k - \mathbf{x}^k))$
- 5: **end for**

Output: \mathbf{x}^N .

Algorithm 3.3 GraRED-P³

Input: Initialization $\mathbf{u}^0 = (\mathbf{x}^0, \mathbf{y}^0) \in \mathbb{R}^n \times \mathbb{R}^n$, iteration number $N > 0$, relaxing parameter $\lambda_k \in [0, 2]$, and $R = I - D_\sigma$ is the residual.

- 1: **for** $k = 0, 1, 2, \dots, N - 1$ **do**
- 2: $\mathbf{d}^k = \text{prox}_{\lambda f}(\mathbf{x}^k - \tau \mathbf{y}^k)$
- 3: $\mathbf{x}^{k+1} = \lambda_k \mathbf{d}^k + (1 - \lambda_k) \mathbf{x}^k$
- 4: $\mathbf{y}^{k+1} = \lambda_k R(\mathbf{y}^k + s(2\mathbf{d}^k - \mathbf{x}^k)) + (1 - \lambda_k) \mathbf{y}^k$
- 5: **end for**

Output: \mathbf{x}^N .

Algorithm 3.4 Relaxed RED-PRO via SD

- 1: **Input:** $\mathbf{x}^0 \in \mathbb{R}^n$, $\{t_k\}_{k \in \mathbb{N}}$, $\alpha \in (0, 1)$, $\lambda, \mu, J, N, \delta > 0$, and the denoiser T .
- 2: **for** $k = 0, 1, 2, \dots, N - 1$ **do**
- 3: $\mathbf{x}^{k,0} = \mathbf{x}^k$
- 4: **for** $j = 0, 1, 2, \dots, J - 1$ **do**
- 5: $\mathbf{x}^{k,j+1} = T_\alpha(t_j \mathbf{x}^k + (1 - t_j) \mathbf{x}^{k,j})$
- 6: **end for**
- 7: $\mathbf{v}^k = \frac{\delta}{\|\mathbf{x}^k - \mathbf{x}^{k,J}\|} \mathbf{x}^k + \left(1 - \frac{\delta}{\|\mathbf{x}^k - \mathbf{x}^{k,J}\|}\right) \mathbf{x}^{k,J}$
- 8: $\mathbf{x}^{k+1} = \mathbf{x}^k - \mu (\nabla f(\mathbf{x}^k) + \lambda(\mathbf{x}^k - \mathbf{v}^k))$
- 9: **end for**
- 10: **Output:** \mathbf{x}^N

3.3.2. Compared with RED-PRO. RED-PRO [20] is defined by

$$(3.7) \quad \min_{\mathbf{x} \in \text{Fix}(T)} \frac{1}{2\sigma^2} \|\mathbf{A}\mathbf{x} - \mathbf{y}\|^2.$$

RED-PRO sheds new insights on the denoiser prior, which theoretically bridges the gap between RED and the PnP prior. However, practical denoisers often have narrow fixed-point sets, leading to suboptimal recovery solutions. To address this issue, they relax the hard constraint of $\text{Fix}(T)$ and replace it with a dilated fixed-point set, defined for some $\delta > 0$ as

$$B_\delta(T) = \{\mathbf{x} \in \mathbb{R}^n : \|\mathbf{x} - P_{\text{Fix}(T)}(\mathbf{x})\| \leq \delta\},$$

where $P_{\text{Fix}(T)}(\mathbf{x})$ is the fixed-point projection of \mathbf{x} onto $\text{Fix}(T)$. The relaxed RED-PRO (RRP) problem is formulated as

$$(3.8) \quad \min_{\mathbf{x} \in \mathbb{R}^n} \frac{1}{2\sigma^2} \|\mathbf{A}\mathbf{x} - \mathbf{y}\|^2 + \frac{\lambda}{2} \|\mathbf{x} - P_{B_\delta(T)}(\mathbf{x})\|^2.$$

Algorithm 3.4 outlines RRP, where $T_\alpha = \alpha T + (1 - \alpha)I$ with the demicontractive denoiser T . When the steepest descent method solves (3.8), it requires an inner loop to calculate the fixed-point projection $P_{\text{Fix}(T)}(\mathbf{x}^k)$, and line 5 in RRP is equivalent to the Halpern iteration.

Comparing Algorithm 3.2 with the inner loop of Algorithm 3.4, we see that both methods share the same algorithmic form of Halpern iteration and utilize identical anchor coefficients. In both cases, finding $P_{\text{Fix}(T)}(\mathbf{x}^k)$ or $P_{\text{Fix}(T)}^{\mathcal{M}}(\mathbf{a})$ corresponds to a bilevel optimization problem that finds the point in the fixed-point set closest to the anchor point \mathbf{x}^k or \mathbf{a} .

The key difference is that HPPP extends Halpern iteration to a degenerate form by employing a positive semidefinite metric \mathcal{M} , whereas the denoiser operator T in RED-PRO is defined under the standard metric $\mathcal{M} = I$. From an optimization perspective, the RRP algorithm is based on gradient descent and uses the classic Halpern iteration in its inner loop. In contrast, \mathcal{T} in GraRED-HP³ is an algorithmic operator and has no inner loop. From a PPP standpoint, we integrate HPPP with denoiser priors to propose Algorithm 3.2.

4. Experiments. In this section, we show the numerical experiments of the algorithms discussed in section 3. First, we will verify the implicit regularity of HPPP by an easy 1D example, and validate the accelerated advantage of HPPP and restarted HPPP by other toy examples. Then, we compare CP, PPP (2.3), GraRED-HP³, and GraRED-P³ for image deblurring and inpainting under the same setting and verify the efficiency of the proposed algorithms. The source code is available at <https://github.com/zsc15/HPPP>.

4.1. A toy example. We consider the optimization problem in \mathbb{R} , i.e.,

$$(4.1) \quad \min_{x \in \mathbb{R}} f(x) + g(x),$$

where $f(x) = \max\{-x, 0\}$ and $g(x) = \max\{1 - x, 0\}$, and we plot $f(x) + g(x)$ in Figure 4.1. The corresponding saddle-point problem is $\min_{x \in \mathbb{R}} \max_{y \in \mathbb{R}} \{xy + f(x) - g^*(y)\}$, where $g^*(y) =$

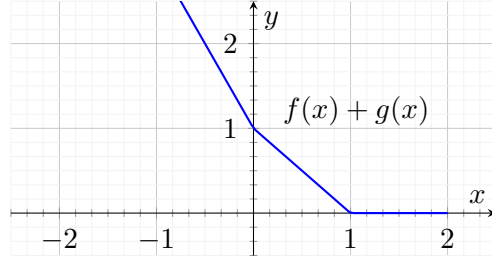


Figure 4.1: The image of $f(x) + g(x)$.

$\max_x [yx - \max\{1 - x, 0\}] = y + \delta_{[-1, 0]}(y)$ and $\delta_{[-1, 0]}$ is the indicator function of the interval $[-1, 0]$. We denote the optimal set $X^* = [1, +\infty) = \arg \min_{x \in \mathbb{R}} f(x) + g(x)$ and the primal-dual objective function $F(x, y) = xy + f(x) - g^*(y)$. Let us solve the saddle-point set $\{(x^*, y^*) : F(x^*, y) \leq F(x^*, y^*) \leq F(x, y^*) \text{ for all } (x, y) \in \mathbb{R}^2\}$ of $F(x, y)$. Fix $x^* \geq 1$; then

$$\max_{-1 \leq y \leq 0} \{x^*y - g^*(y)\} = \max_{-1 \leq y \leq 0} \{x^*y - y\} = \begin{cases} 0, & x^* > 1, y = 0, \\ 0, & x^* = 1, y \in [-1, 0]. \end{cases}$$

If $x^* = 1$, assume that $-1 \leq y^* < 0$, then $F(1, y^*) = 0$, while $F(x, y^*) = y^*(x - 1) + \max\{-x, 0\}$, and there exists $x = 2$ such that $F(2, y^*) = y^* < F(1, y^*)$, which leads to a contradiction. Therefore, the saddle-point set is $\Omega = \{(x^*, y^*) : x^* \geq 1, y^* = 0\}$.

When $\mathcal{M} = \begin{pmatrix} 1 & -1 \\ -1 & 1 \end{pmatrix}$, as shown in Figure 4.2, the minimization $\arg \min_{\mathbf{u} \in \text{Fix}(\mathcal{T})} \|\mathbf{u} - \mathbf{a}\|_{\mathcal{M}}^2 = \arg \min_{(x,y) \in \Omega} (x - x_a - (y - y_a))^2$ can be interpreted as finding the \mathcal{M} -projection, namely, the projection of the anchor point $\mathbf{a} = (x_a, y_a)$ onto the line $x - y = x_a - y_a$. Therefore, the \mathcal{M} -projection of \mathbf{a} onto Ω is uniquely determined,

$$(4.2) \quad P_{\Omega}^{\mathcal{M}}(\mathbf{a}) = \begin{cases} (1, 0), & x_a - y_a - 1 \leq 0, \\ (x_a - y_a, 0), & x_a - y_a - 1 > 0. \end{cases}$$

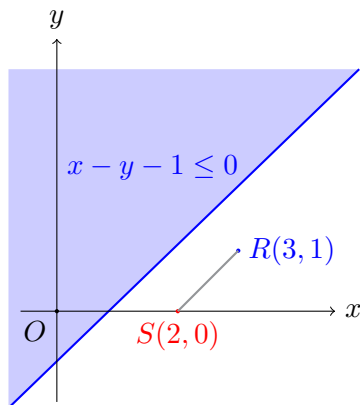


Figure 4.2: \mathcal{M} -projection onto the saddle-point set.

We set the total iteration number $N = 1000$. As shown in Figure 4.3a, with the anchor point fixed at $\mathbf{a} = (12, 9)$, the sequence $\mathbf{u}^k = (x^k, y^k)$ generated by HPPP converges to the same point $\mathbf{u}^* = (3, 0)$, regardless of the initial point, which verifies Proposition 3.2 and (4.2). HPPP is also an implicitly regularized method. In contrast, Figure 4.3b shows that the sequence generated by PPP oscillates around the limit $(1.8, 0)$. However, a quantitative mathematical characterization of the limit of the PPP sequence remains elusive.

4.2. A 2D toy example. We consider a $\frac{1}{\gamma}$ -contractive operator $T_{\theta} : \mathbb{R}^2 \rightarrow \mathbb{R}^2$ from [41] for any $\mathbf{x} = (x_1, x_2)^{\text{T}} \in \mathbb{R}^2$,

$$T_{\theta} \mathbf{x} = \frac{1}{\gamma} \begin{pmatrix} \cos \theta & -\sin \theta \\ \sin \theta & \cos \theta \end{pmatrix} \mathbf{x}.$$

We compare the Picard iteration $\mathbf{x}^{k+1} = T_{\theta} \mathbf{x}^k$, PPP ($\lambda_k = 0.1$), HPPP ($\mu_k = \frac{1}{k+1}$), and restarted HPPP ($q = 50$). Set $\mathcal{A} = \begin{pmatrix} -T_{\theta} & I \\ -I & I \end{pmatrix}$ and $\mathcal{M} = \begin{pmatrix} \frac{1}{\tau} I & -I \\ -I & \frac{1}{s} I \end{pmatrix}$ with $\tau = 0.8, s = 1.25$, and initial points $\mathbf{x}^0 = \mathbf{y}^0 = \mathbf{x}_a = \mathbf{y}_a = (1, 0)^{\text{T}}$, where $\mathbf{a} = \mathbf{u}^0$. Figure 4.4 shows that HPPP and restarted HPPP indeed provide accelerated residual decay.

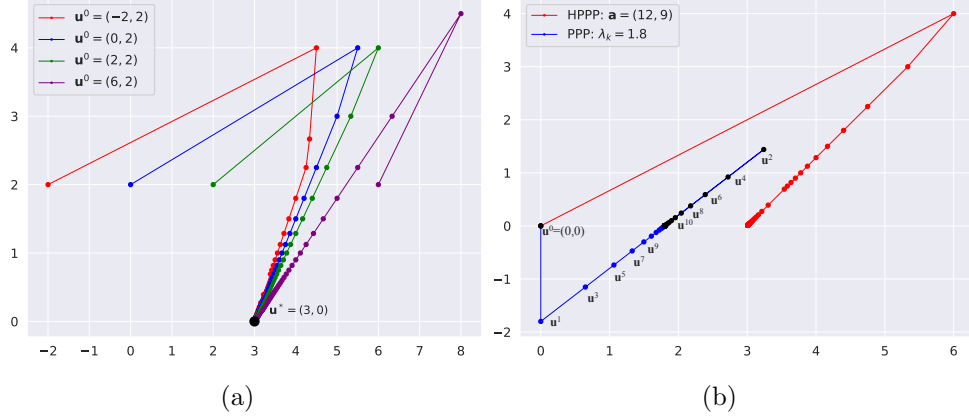


Figure 4.3: Trajectory of $\mathbf{u}^k = (x^k, y^k)$ generated by HPPP or PPP.

4.3. An infinite-dimensional example. We consider an infinite-dimensional problem on ℓ^2 from [7], the space of square summable sequences. For any $\mathbf{x} = (x_0, x_1, x_2, \dots) \in \ell^2$, the norm is $\|\mathbf{x}\| = \left(\sum_{k \in \mathbb{N}} |x_k|^2\right)^{\frac{1}{2}}$. We consider the following operator inclusion problem:

$$(4.3) \quad \mathbf{0} \in \mathcal{A}_1 \mathbf{x} + \mathcal{A}_2 \mathbf{x}, \mathcal{A}_1 = -\mathcal{S} - \mathbf{b}, \mathcal{A}_2 = I,$$

where $\mathcal{S}(\mathbf{x}) = (0, x_0, x_1, \dots)$ is the right-shift operator and $\mathbf{b} = (1, -1, 0, \dots)$. Since $\mathcal{A}_1, \mathcal{A}_2$ are nonexpansive, $\mathcal{A}_1, \mathcal{A}_2$ are maximal monotone [2, Example 20.29]. Additionally, by solving the above inclusion problem (4.3), we obtain $\mathbf{x}^* = (1, 0, \dots)$. Using $\mathcal{A} = \begin{pmatrix} \mathcal{A}_1 & I \\ -I & I \end{pmatrix}$ and positive semidefinite preconditioner $\mathcal{M} = \begin{pmatrix} 2I & -I \\ -I & \frac{1}{2}I \end{pmatrix}$, we compare the PPP iteration with $\lambda_k = 0.5, 1, 1.8$. We set $N = 10^3, \tau = 0.5, s = 2$ and initialize $\mathbf{x}^0 = (0.9, 1, 0, \dots)$ for HPPP and PPP, and the anchor point is the same as the initial point, i.e., $\mathbf{a} = (\mathbf{x}^0, \mathbf{x}^0)$. For this example, we present visual results about the residual and the distance to the solution. As illustrated in Figure 4.5, HPPP outperforms PPP in terms of both $\|\mathbf{x}^k - \mathbf{x}^*\|$ and $\|\mathbf{u}^{k+1} - \mathbf{u}^k\|$.

4.4. Image deblurring. First, we compared CP [16], PPP [9], and HPPP for TV-regularized IR problems. For TV-regularized IR problems,

$$(4.4) \quad \min_{\mathbf{x} \in \mathbb{R}^n} \frac{\lambda}{2} \|\mathbf{A}\mathbf{x} - \mathbf{y}\|_2^2 + \beta \|\nabla \mathbf{x}\|_1,$$

where \mathbf{y} is the degraded image, \mathbf{A} is a linear operator, and λ, β are balance coefficients.

We use a 2D Gaussian function with a standard deviation of 1.6 to convolve 10 test grayscale images, and finally obtain the degraded images with an additive white Gaussian noise with the noise level $\sigma = 2.55$. Firstly, we compared three algorithms, CP, PPP, and the proposed HPPP. All the algorithms use the degraded images as initial points. We calculate the norm $K = \|\nabla\| = 1.75$, and choose the total iteration $N = 400$, balance coefficients

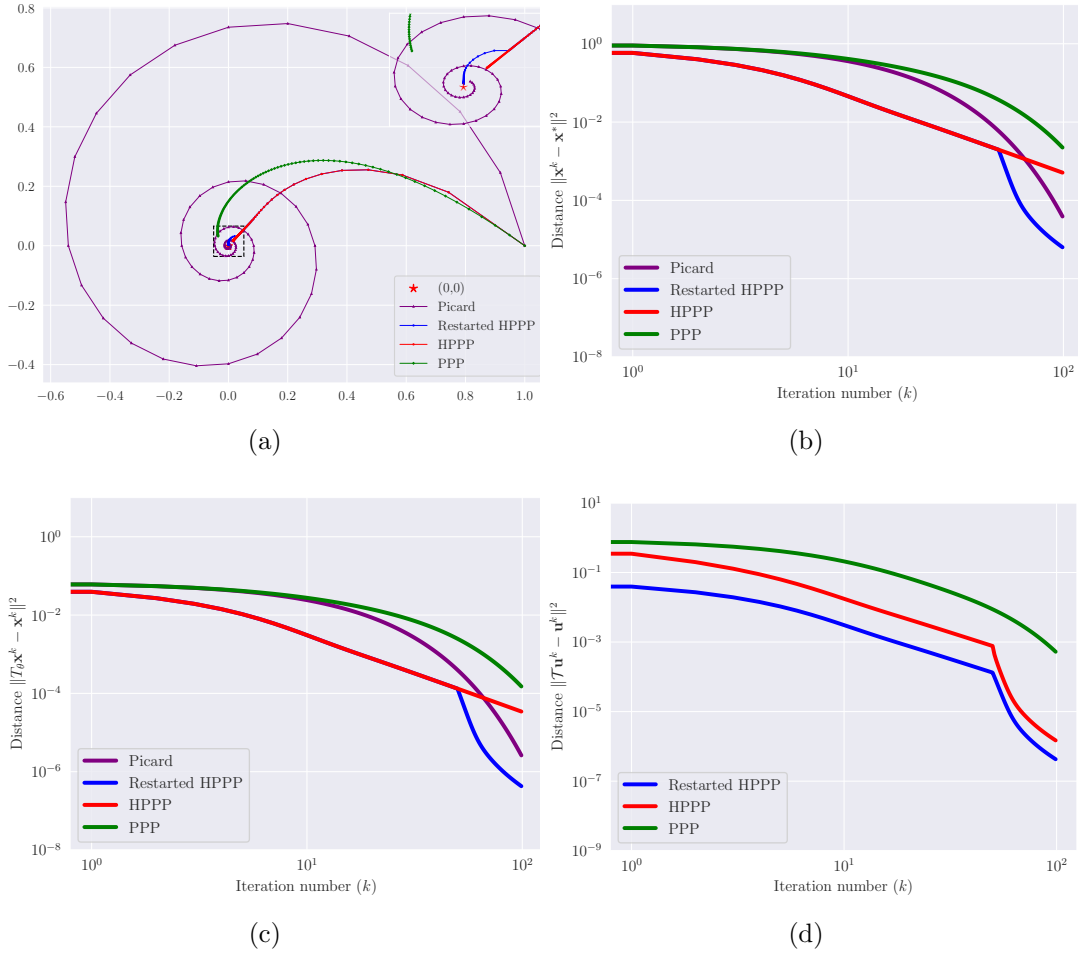


Figure 4.4: Trajectories, distance to solution, and two residuals of iterates for the 2D toy example. Here $\gamma = 1/0.95$, $\theta = 15^\circ$, $N = 100$.

$\lambda = 2$, $\beta = 5 \times 10^{-4}$. Their parameters are given in Table 4.1. Both GraRED-P³ and GraRED-HP³ use DnCNN; other parameters are used as follows:

- GraRED-P³ : $\tau = 1$, $s = 1$, $\lambda_k = 0.2$, $\lambda = 20$;
- GraRED-HP³ : $\tau = 1$, $s = 1$, $\mu_k = 1/(k + 2)$, $\lambda = 20$, $\mathbf{x}_a = \mathbf{y}$, $\mathbf{y}_a = \mathbf{0}$.

Table 4.2 shows PSNR (dB) of restoration results on CP, PPP, HPPP, GraRED-P³, and GraRED-HP³. The performance of these methods is evaluated using PSNR measure. The best recovery results are highlighted in bold. From Table 4.2, GraRED-P³ and GraRED-HP³ are better than classic algorithms with explicit TV regularization, which demonstrates that the implicit regularizer is more powerful for regularizing inverse imaging problems. We visualize the numerical comparison between GraRED-P³, GraRED-HP³, CP, PPP, and HPPP in Figure 4.6. We further compare the robustness of the initial points between the proposed

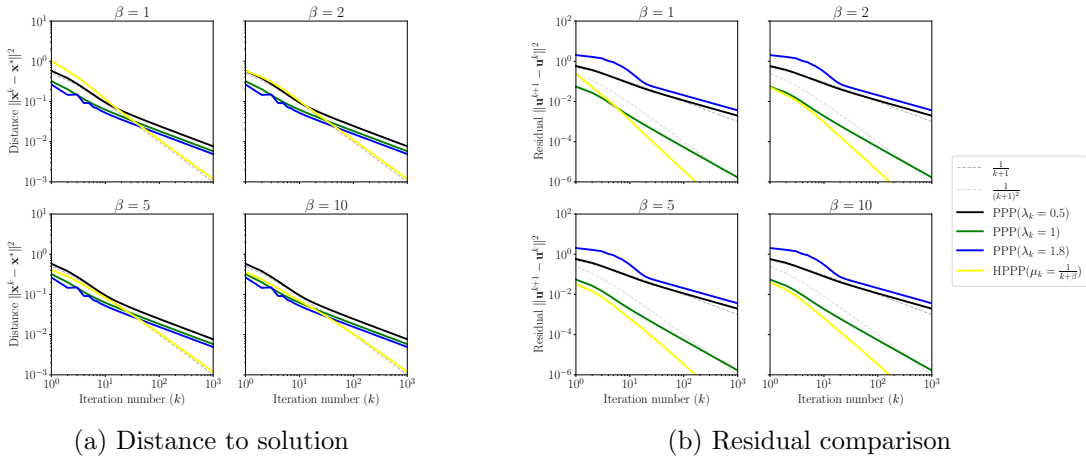


Figure 4.5: Comparison with PPP to solve an infinite-dimensional problem in ℓ^2 space.

HPPP, CP, and PPP with TV regularization. As shown in Figure 4.7, we plot their respective evolutions of PSNR values for iterations for **Butterfly** and **Parrots** with 10 different random initial points, here we choose the degraded image \mathbf{y} as the anchor point. Once the anchor point is chosen, the proposed HPPP algorithm is robust to random perturbations of the initial points, which achieves stable recovery.

Table 4.1: Parameters on CP, PPP, and HPP with TV regularization for image deblurring.

CP	$\tau = s = 1/K = 0.57$
PPP	$\tau = s = 1/K = 0.57, \lambda_k = 1.95$ or $\lambda_k = 1.2$
HPPP	$\tau = s = 1/K = 0.57, \mu_k = \frac{1}{k+2}, \mathbf{x}_a = \mathbf{A}^T \mathbf{y}, \mathbf{y}_a = 0 \cdot \nabla \mathbf{x}_a$

Table 4.2: Deblurring results of grayscale images compared with CP, PPP, and HPPP about the Gauss blurring kernel.

	Cameraman	House	Pepper	Starfish	Butterfly	Craft	Parrots	Barbara	Boat
CP	26.04	30.86	25.99	27.53	27.85	25.51	26.88	24.46	28.99
PPP	26.05	30.85	25.99	27.53	27.85	25.51	26.88	24.46	28.98
HPPP	26.00	31.39	26.05	27.65	27.99	25.51	26.82	24.51	29.09
GraRED-P ³	26.87	32.51	28.34	29.16	29.70	26.90	27.95	24.66	29.68
GraRED-HP ³	26.85	32.51	28.80	29.15	29.67	27.03	27.89	24.66	29.99

Second, we compared RED and RED-PRO. Following [47, 20], a 9×9 uniform point spread function (PSF) and a 2D Gaussian function with a standard deviation of 1.6 are used to convolve test images. We finally obtained the degraded images with the noise level $\sigma = \sqrt{2}$. The original RGB image is converted into the YCbCr image, all algorithms are applied to the luminance channel, and then the reconstruction image is returned to RGB space to obtain the

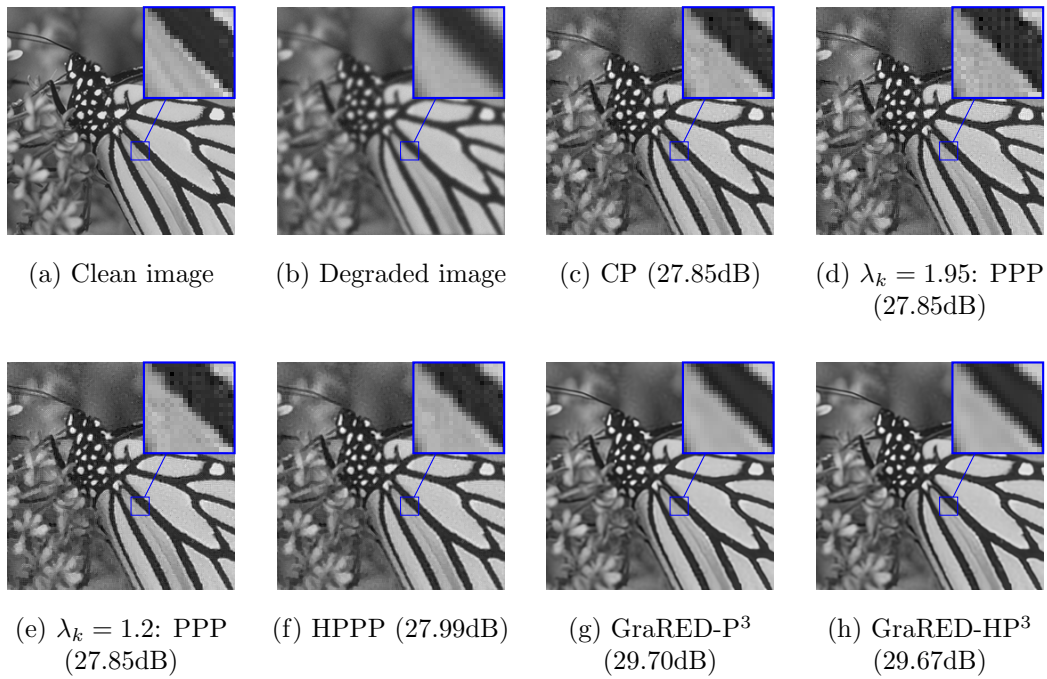


Figure 4.6: Deblurring results of **Butterfly** degraded by the Gaussian blur kernel with noise level $\sigma = 2.55$.

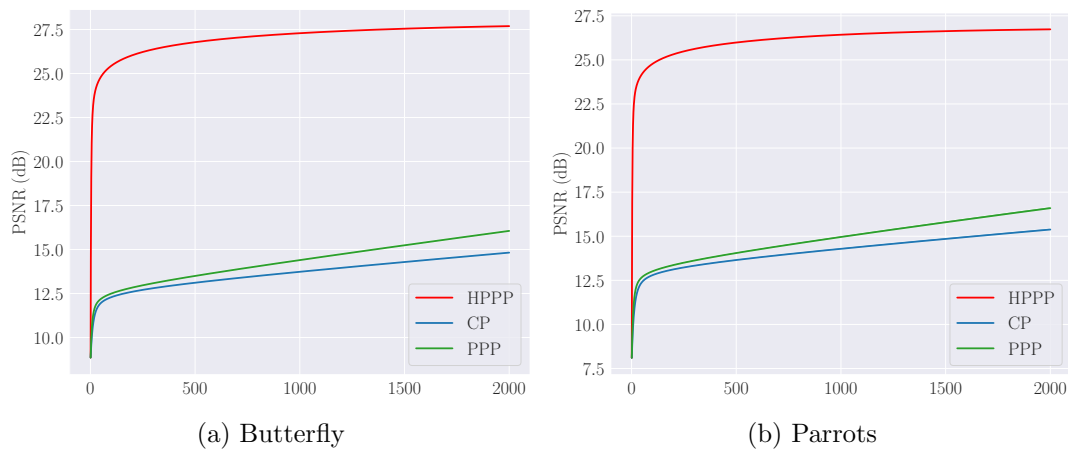


Figure 4.7: Robustness comparison with random initialization. Test images are degraded by the Gaussian blurring kernel with the noise level $\sigma = 2.55$.

final image. PSNR is measured on the luminance channel of the ground truth and the restored images. Table 4.3 shows the PSNR values of the restoration results on RED, RED-PRO, RRP, GraRED-P³, and GraRED-HP³. From the deblurring experiment of Table 4.3 and Figure 4.9, GraRED-P³ and GraRED-HP³ achieve better performance than RED, RED-PRO, and RRP, which illustrates that KM or Halpern iteration used in PPP methods is effective. We further compare the differences among GraRED-P³, GraRED-HP³, and restarted HPPP under six different settings with $\lambda = 40, \tau = s = 1, \lambda_k = 0.2, \mu_k = \frac{1}{k+1}, N = 500, q = 100$. In Table 4.5, we report the average PSNR values of 15 test images using six different blur kernels. When the anchor point and the initial point coincide, GraRED-HP³ achieves the best performance on some IR tasks. Moreover, by dynamically updating the anchor points, restarted HPPP further boosts the performance of GraRED-HP³.

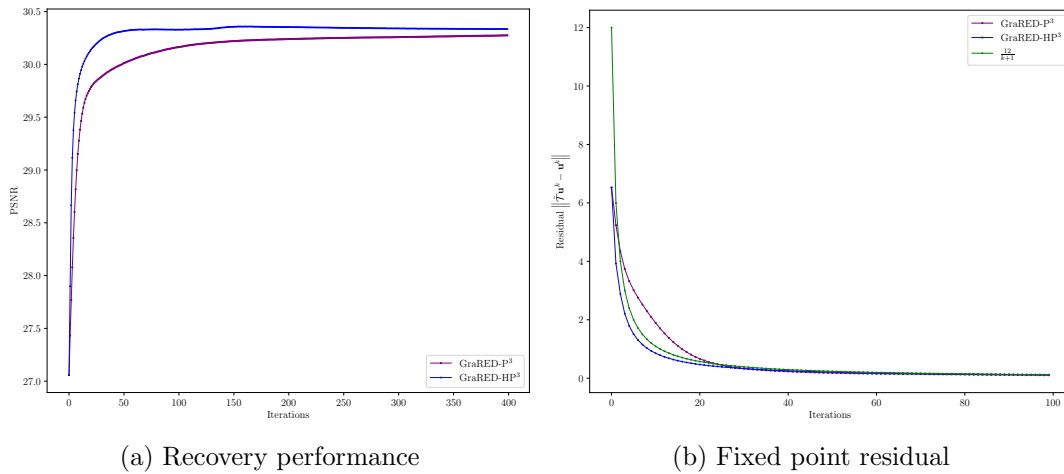


Figure 4.8: Recovery performance and fixed-point residual comparison for the House image degraded by the Gaussian blurring kernel with the noise level $\sigma = 5$. Here D_1 is used.

Additionally, we trained a FNE-DnCNN (D_1) using real spectral normalization [49], which is employed in RED and RED-PRO. We also compared our results with state-of-the-art methods using advanced denoisers, such as DRUNet (D_2) [65] and GS (D_3) [32, 33]. The PnP-DYS method [59] uses the Davis-Yin splitting (DYS) algorithm. For GraRED-HP³, the anchor point is the same as the initial point. The default parameters are presented in Table 4.4. As shown in Table 4.6, Restarted HPPP with advanced denoisers achieves competitive or even superior performance compared to state-of-the-art methods. In Figure 4.8, we compare GraRED-P³ ($\lambda_k = 0.1$) and GraRED-HP³ ($\mathbf{a} = \mathbf{u}^0, \mu_k = \frac{1}{k+1}$). The results demonstrate that GraRED-HP³ achieves better recovery performance and exhibits a faster fixed-point convergence rate than GraRED-P³.

4.5. Image inpainting. In this section, we use the proposed algorithm to solve TV-regularized image inpainting problems and compare their numerical results with CP [16],

Table 4.3: Recovery results are obtained by different algorithms with trainable nonlinear reaction-diffusion (TNRD) denoiser [18]. The best two results are highlighted in red and blue, respectively.

Algorithms	Uniform kernel				Gaussian kernel($\sigma_k = 1.6$)			
	Bike	Butterfly	Flower	Hat	Bike	Butterfly	Flower	Hat
RED [47]	26.10	30.41	30.18	32.16	27.90	31.66	32.05	33.30
RED-PRO(HSD) [20]	24.95	27.24	29.38	31.55	27.36	30.55	31.81	33.07
RRP [20]	26.48	30.64	30.46	32.25	28.02	31.66	32.08	33.26
GraRED-P ³	26.55	30.72	30.67	32.43	28.13	31.81	32.42	33.51
GraRED-HP ³	26.80	30.88	30.74	32.42	28.06	31.80	32.27	33.50

Table 4.4: Parameters on GraRED-HP³ and restarted HPPP with advanced denoisers.

GraRED-HP ³ (D_1)	$\tau = 3, s = 1/3, N = 500$
Restarted HPPP(D_2)	$\tau = 1.2, s = 1/1.2, N = 30, q = 10$
GraRED-HP ³ (D_3)	$\tau = 1.8, s = 1/1.8, N = 500$
Restarted HPPP ³ (D_3)	$\tau = 1.8, s = 1/1.8, N = 500, q = 40$

PPP [9], and HPPP algorithms. The discrete image inpainting model is

$$\min_{\mathbf{x} \in \mathbb{R}^n} \lambda \|\mathbf{M} \odot \mathbf{x} - \mathbf{y}\|_F^2 + \beta \|\nabla \mathbf{x}\|_1,$$

where \mathbf{y} is the degraded image, \mathbf{M} is a mask, and λ, β are balance coefficients.

We test 10 common images for evaluation. The first \mathbf{M} is filled with a Bernoulli random mask, where each pixel is missing with probability $p = 0.5$, i.e., 50% of pixels are missed. The second \mathbf{M} is a character mask where about 19% of pixels are missed. All the algorithms start with the degraded image. For classic algorithms, we fix the balance parameter $\alpha = 0.01$ and the total number $N = 400$ and use the following additional parameters:

- HPPP: $\tau = s = 1/\|K\| = 0.57, \mathbf{x}_a = \mathbf{1} \in \mathbb{R}^{m \times n}, \mathbf{y}_a = 0 \cdot \nabla \mathbf{x}_a, \mu_k = \frac{1}{10(k+2)}$;
- PPP: $\tau = s = 1/\|K\| = 0.57, \lambda_k = 1.6$, or $\lambda_k = 1.2$;
- CP: $\tau = s = 1/\|K\| = 0.57$.

Both GraRED-P³ and GraRED-HP³ use DnCNN [49], other parameters are used:

- GraRED-P³: $\tau = 10, s = 0.1, \lambda_k = 0.2, \lambda = 5$;
- GraRED-HP³: $\tau = 10, s = 0.1, \mu_k = 0.05/(k+2), \lambda = 5, \mathbf{x}_a = \mathbf{y}, \mathbf{y}_a = \mathbf{0}$.

In Tables 4.7 and 4.8, we compared the numerical performance of classic algorithms with TV regularization. In Figures 4.10 and 4.11, we compare visualization results of **House** degraded by the Bernoulli random mask and the character mask; the proposed algorithms achieve better visual performance than TV regularization.

5. Conclusions. This paper introduces a Halpern-type PPP (HPPP) algorithm, which has the advantage of strong convergence over PPP. In addition, GraRED-HP³ is proposed by integrating HPPP with denoiser priors for IR problems, which is an accelerated PnP-ADMM. Advantages of HPPP are demonstrated through several toy examples, and GraRED-HP³ achieves state-of-the-art performance on IR experiments. In the future, we plan to extend the definition of \mathcal{M} -monotonicity to \mathcal{M} -comonotonicity for nonconvex case [4].

Table 4.5: Comparison with GraRED-P³, GraRED-HP³, and restarted HPPP with TNRD for different tasks.

Kernels						
noise level, scale	$\sigma = 5, \times 3$	$\sigma = 2.55, \times 1$	$\sigma = 2.55, \times 1$			
GraRED-P ³	27.49	29.25	30.92	28.19	33.53	33.73
GraRED-HP ³	27.61	29.33	30.99	28.32	33.53	33.71
Restarted HPPP	27.66	29.36	31.00	28.34	33.53	33.73

Table 4.6: Comparison with state-of-the-art methods. Test grayscale images are degraded by the Gaussian kernel with the noise level $\sigma = 2.55$. The best two results are highlighted in red and blue, respectively.

	Pepper	Craft	Cameraman	Couple	Man	House	Starfish	Butterfly	Boat
RED [47]	27.19	26.00	26.46	29.21	30.16	32.41	28.46	28.36	29.58
RED-PRO [20]	27.43	26.05	26.39	28.99	29.98	32.41	28.25	28.21	29.38
DPIR [65]	28.47	27.02	27.63	30.24	30.89	33.56	29.62	30.43	30.54
PnP-DRS [33]	29.79	26.92	27.46	29.70	29.59	33.25	29.94	30.66	29.46
PnP-PGD [32]	27.18	26.28	26.73	29.17	29.14	32.84	29.14	29.87	30.37
PnP-DYS [59]	27.22	26.27	26.62	28.97	29.04	32.87	29.06	29.88	28.68
GraRED-HP ³ (D ₁)	29.11	27.05	27.16	29.37	30.46	32.43	28.77	29.51	29.86
Restarted HPPP(D ₂)	28.34	26.75	27.02	29.71	30.44	32.69	28.91	29.28	30.01
GraRED-HP ³ (D ₃)	29.51	27.09	27.45	30.03	30.79	33.15	30.06	30.49	30.36
Restarted HPPP(D ₃)	29.81	27.13	27.49	30.04	30.80	33.15	30.09	30.53	30.37

Table 4.7: Numerical results of image inpainting compared with CP, PPP, and HPPP (noise level $\sigma = 2.55$, Bernoulli random missing).

	Cameraman	House	Peppers	Starfish	Butterfly	Craft	Parrots	Barbara	Boat
CP	23.54	28.94	24.53	23.89	23.59	23.42	23.20	23.10	26.29
PPP	23.58	29.05	24.53	24.32	23.76	23.43	23.33	23.13	26.36
HPPP	23.89	29.19	24.55	24.46	24.04	23.52	23.44	23.35	26.45
GraRED-P ³	29.92	36.15	32.67	31.99	31.95	29.53	30.05	32.25	32.91
GraRED-HP ³	29.90	36.14	32.68	31.97	31.92	29.52	30.04	32.23	32.90

Table 4.8: Numerical results of image inpainting compared with CP, PPP, and HPPP (noise level $\sigma = 2.55$, character texture missing).

	Cameraman	House	Peppers	Starfish	Butterfly	Craft	Parrots	Barbara	Boat
CP	25.87	31.58	29.40	26.16	25.60	26.33	25.20	24.21	25.23
PPP	26.33	31.78	30.13	26.86	26.08	26.47	25.64	27.32	28.05
HPPP	26.33	32.00	30.02	26.88	26.38	26.51	25.83	27.34	28.09
GraRED-P ³	29.18	37.46	33.79	30.89	29.45	29.20	26.04	29.68	30.04
GraRED-HP ³	29.13	37.47	33.80	30.93	29.42	29.20	26.02	29.60	30.04



Figure 4.9: Deblurring results of **Butterfly** degraded by the uniform kernel.

Acknowledgments. The authors thank Prof. Defeng Sun for bringing the interesting work [52] to our attention and Mr. Feng Xue for his insightful discussions. We sincerely appreciate Associate Editor Michael Elad and the anonymous referees for their thorough review and valuable comments, which have substantially improved this paper.

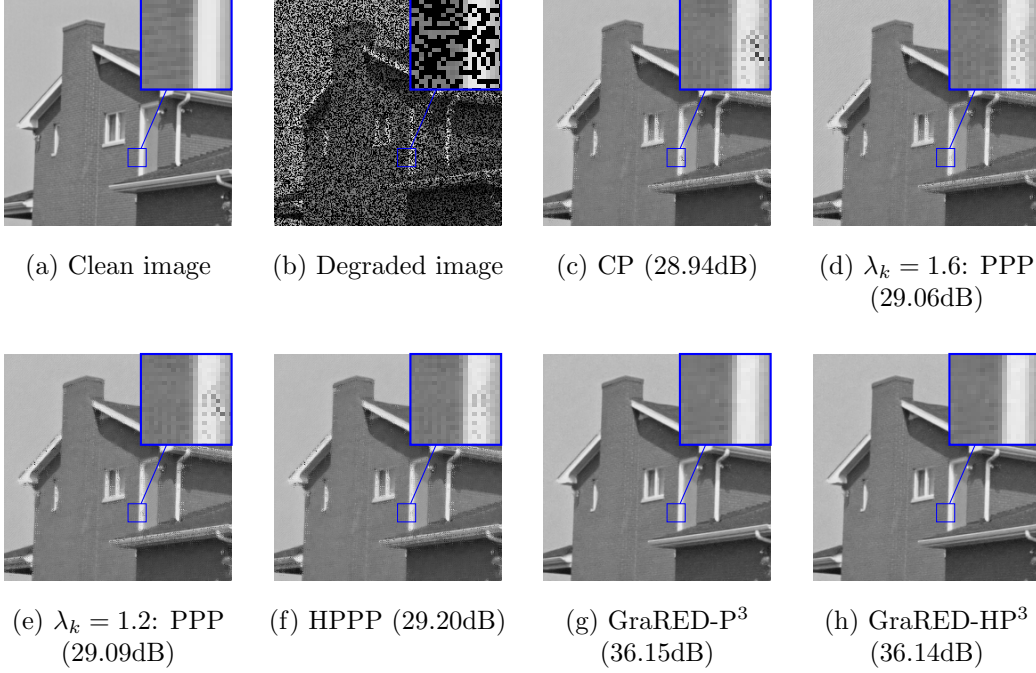


Figure 4.10: Recovery results of **House** degraded by the random mask.

Appendix A. Boundedness. First, we study the boundedness and asymptotic regularity of $\{\mathbf{u}^k\}_{k \in \mathbb{N}}$ generated by (1.5). To further establish regularity of $\{\mathbf{u}^k\}_{k \in \mathbb{N}}$ (Theorem 3.1), we introduce an important lemma from [30, Lemma 2.5].

Lemma A.1. *Let $\{a_k\}_{k \in \mathbb{N}}$ be a sequence of non-negative real numbers satisfying*

$$(A.1) \quad a_{k+1} \leq (1 - \mu_k)a_k + \mu_k\beta_k + \gamma_k,$$

where $\{\mu_k\}_{k \in \mathbb{N}}, \{\beta_k\}_{k \in \mathbb{N}}, \{\gamma_k\}_{k \in \mathbb{N}}$ satisfies the following conditions:

- (i) $\{\mu_k\}$ converges to 0 in $[0, 1]$, and $\sum_{k=0}^{\infty} \mu_k = +\infty$, or equivalently, $\prod_{k=0}^{\infty} (1 - \mu_k) = 0$;
- (ii) $\limsup_{k \rightarrow \infty} \beta_k \leq 0$;
- (iii) $\gamma_k \geq 0$, $\sum_{k=0}^{\infty} \gamma_k < \infty$.

Then $\lim_{k \rightarrow \infty} a_k = 0$.

Lemma A.2. *Let $\mathcal{A} : \mathcal{H} \rightarrow 2^{\mathcal{H}}$ be an operator with $\text{zer}\mathcal{A} \neq \emptyset$, and let \mathcal{M} be an admissible preconditioner such that $\mathcal{M}^{-1}\mathcal{A}$ is \mathcal{M} -monotone and $(\mathcal{M} + \mathcal{A})^{-1}$ is L -Lipschitz. Let $\{\mathbf{u}^k\}_{k \in \mathbb{N}}$ be the sequence generated by (1.5). Then the following assertions are hold:*

- (i) *The sequences $\{\mathbf{u}^k\}_{k \in \mathbb{N}}, \{\mathcal{T}\mathbf{u}^k\}_{k \in \mathbb{N}}$ are bounded;*
- (ii) *If the sequence $\{\mu_k\}_{k \in \mathbb{N}}$ satisfies $\lim_{k \rightarrow \infty} \frac{\mu_{k+1} - \mu_k}{\mu_k} = 0$ or $\sum_{k \in \mathbb{N}} |\mu_{k+1} - \mu_k| < \infty$, then $\lim_{k \rightarrow \infty} \|\mathcal{T}\mathbf{u}^k - \mathbf{u}^k\|_{\mathcal{M}} = 0$;*
- (iii) *If the conditions of (ii) hold, then $\lim_{k \rightarrow \infty} \|\mathbf{u}^{k+1} - \mathbf{u}^k\| = 0, \lim_{k \rightarrow \infty} \|\mathcal{T}\mathbf{u}^k - \mathbf{u}^k\| = 0$.*

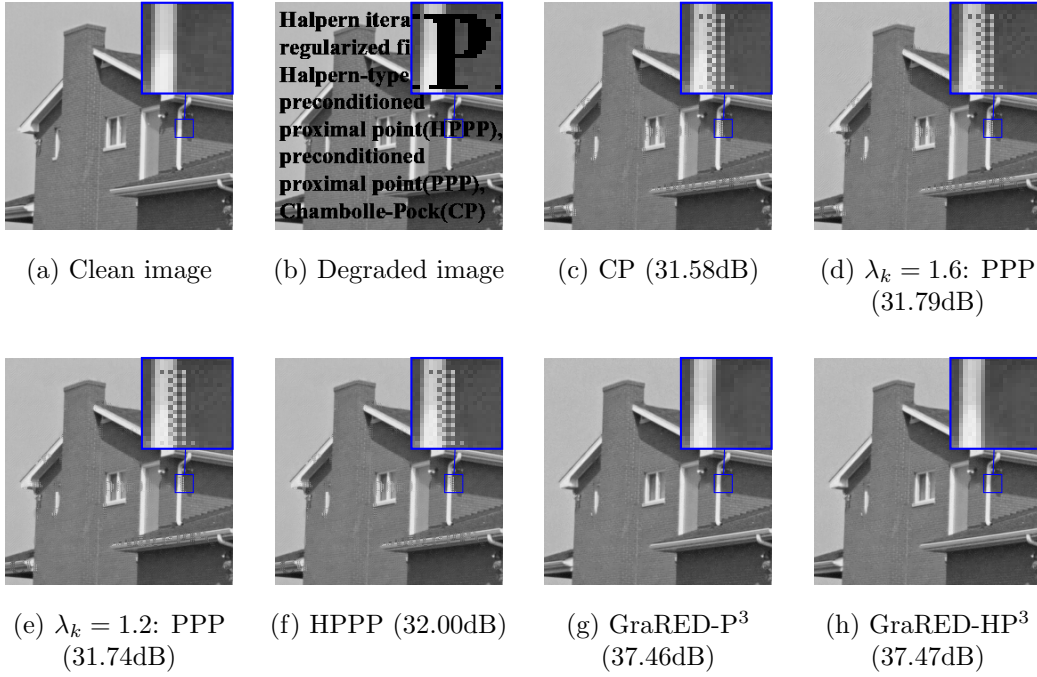


Figure 4.11: Recovery results of **House** degraded by the character mask.

Proof. Let $\mathcal{M} = \mathcal{C}\mathcal{C}^*$ be a decomposition of \mathcal{M} [9, Proposition 2.3]. Denote

$$(A.2) \quad C = L \|\mathcal{C}\|,$$

for $\mathbf{u}', \mathbf{u}'' \in \mathcal{H}$, we have

$$(A.3) \quad \begin{aligned} \|\mathcal{T}\mathbf{u}' - \mathcal{T}\mathbf{u}''\| &= \|(\mathcal{M} + \mathcal{A})^{-1}\mathcal{C}\mathcal{C}^*\mathbf{u}' - (\mathcal{M} + \mathcal{A})^{-1}\mathcal{C}\mathcal{C}^*\mathbf{u}''\| \\ &= \|(\mathcal{M} + \mathcal{A})^{-1}\mathcal{C}(\mathcal{C}^*\mathbf{u}' - \mathcal{C}^*\mathbf{u}'')\| \\ &\leq L \|\mathcal{C}\| \|\mathcal{C}^*(\mathbf{u}' - \mathbf{u}'')\| \\ &= L \|\mathcal{C}\| \|\mathbf{u}' - \mathbf{u}''\|_{\mathcal{M}} \\ &= C \|\mathbf{u}' - \mathbf{u}''\|_{\mathcal{M}}, \end{aligned}$$

where the third inequality follows from the L -Lipschitz property of $(\mathcal{M} + \mathcal{A})^{-1}$, and the fourth equality follows from the definition of $\|\mathbf{u}\|_{\mathcal{M}}$, i.e., $\|\mathbf{u}\|_{\mathcal{M}} = \sqrt{\langle \mathcal{M}\mathbf{u}, \mathbf{u} \rangle} = \|\mathcal{C}^*\mathbf{u}\|$ for any $\mathbf{u} \in \mathcal{H}$.

First, we prove $\{\mathbf{u}^k\}_{k \in \mathbb{N}}$ is bounded. For any $\mathbf{u}^* \in \text{Fix}(\mathcal{T})$, we have

$$\begin{aligned} \left\| \mathbf{u}^{k+1} - \mathbf{u}^* \right\|_{\mathcal{M}} &= \left\| \mu_{k+1}(\mathbf{a} - \mathbf{u}^*) + (1 - \mu_{k+1})(\mathcal{T}\mathbf{u}^k - \mathbf{u}^*) \right\|_{\mathcal{M}} \\ &\leq \mu_{k+1} \|\mathbf{a} - \mathbf{u}^*\|_{\mathcal{M}} + (1 - \mu_{k+1}) \left\| \mathbf{u}^k - \mathbf{u}^* \right\|_{\mathcal{M}} \\ &\leq \max\{\|\mathbf{a} - \mathbf{u}^*\|_{\mathcal{M}}, \left\| \mathbf{u}^k - \mathbf{u}^* \right\|_{\mathcal{M}}\} \\ &\leq \dots \leq \max\{\|\mathbf{a} - \mathbf{u}^*\|_{\mathcal{M}}, \left\| \mathbf{u}^0 - \mathbf{u}^* \right\|_{\mathcal{M}}\}. \end{aligned}$$

Denote

$$(A.4) \quad C_1 = \max\{\|\mathbf{a} - \mathbf{u}^*\|_{\mathcal{M}}, \left\| \mathbf{u}^0 - \mathbf{u}^* \right\|_{\mathcal{M}}\},$$

then we have $\left\| \mathbf{u}^k - \mathbf{u}^* \right\|_{\mathcal{M}} \leq C_1$ for all $k \in \mathbb{N}$.

Furthermore,

$$\begin{aligned} \left\| \mathbf{u}^{k+1} - \mathbf{u}^* \right\| &\leq \mu_{k+1} \|\mathbf{a} - \mathbf{u}^*\| + (1 - \mu_{k+1}) \left\| \mathcal{T}\mathbf{u}^k - \mathbf{u}^* \right\| \\ &\leq \mu_{k+1} \|\mathbf{a} - \mathbf{u}^*\| + (1 - \mu_{k+1}) \cdot C \left\| \mathbf{u}^k - \mathbf{u}^* \right\|_{\mathcal{M}} \\ &\leq \max\{\|\mathbf{a} - \mathbf{u}^*\|, CC_1\} < +\infty. \end{aligned}$$

By (A.3), we have

$$(A.5) \quad \left\| \mathcal{T}\mathbf{u}^k - \mathbf{u}^* \right\| \leq C \left\| \mathbf{u}^k - \mathbf{u}^* \right\|_{\mathcal{M}} \leq CC_1 < +\infty.$$

So the sequence $\{\mathcal{T}\mathbf{u}^k\}_{k \in \mathbb{N}}$ is also bounded.

For (ii), we will prove $\lim_{k \rightarrow \infty} \left\| \mathcal{T}\mathbf{u}^k - \mathbf{u}^* \right\|_{\mathcal{M}} = 0$. Let $M = \|\mathbf{a} - \mathbf{u}^*\|_{\mathcal{M}} + C_1$, by the triangle inequality and the \mathcal{M} -non-expansiveness of \mathcal{T} , we have

$$\begin{aligned} \left\| \mathbf{a} - \mathcal{T}\mathbf{u}^k \right\|_{\mathcal{M}} &\leq \|\mathbf{a} - \mathbf{u}^*\|_{\mathcal{M}} + \left\| \mathbf{u}^* - \mathcal{T}\mathbf{u}^k \right\|_{\mathcal{M}} \\ &\leq \|\mathbf{a} - \mathbf{u}^*\|_{\mathcal{M}} + \left\| \mathbf{u}^k - \mathbf{u}^* \right\|_{\mathcal{M}} \\ (A.6) \quad &\leq \|\mathbf{a} - \mathbf{u}^*\|_{\mathcal{M}} + C_1 = M. \end{aligned}$$

Note that by $\mathbf{u}^{k+1} = \mu_{k+1}\mathbf{a} + (1 - \mu_{k+1})\mathcal{T}\mathbf{u}^k$, we have

$$\begin{aligned} \left\| \mathbf{u}^{k+1} - \mathbf{u}^k \right\|_{\mathcal{M}} &= \left\| (\mu_{k+1} - \mu_k)(\mathbf{a} - \mathcal{T}\mathbf{u}^{k-1}) + (1 - \mu_{k+1})(\mathcal{T}\mathbf{u}^k - \mathcal{T}\mathbf{u}^{k-1}) \right\|_{\mathcal{M}} \\ &\leq (1 - \mu_{k+1}) \left\| \mathcal{T}\mathbf{u}^k - \mathcal{T}\mathbf{u}^{k-1} \right\|_{\mathcal{M}} + |\mu_{k+1} - \mu_k| \left\| \mathbf{a} - \mathcal{T}\mathbf{u}^{k-1} \right\|_{\mathcal{M}} \\ (A.7) \quad &\leq (1 - \mu_{k+1}) \left\| \mathbf{u}^k - \mathbf{u}^{k-1} \right\|_{\mathcal{M}} + M |\mu_{k+1} - \mu_k|, \end{aligned}$$

where the last inequality follows from Lemma 2.3 and (A.6).

Applying Lemma A.1 together with $\lim_{k \rightarrow \infty} \frac{\mu_{k+1} - \mu_k}{\mu_k} = 0$ or $\sum_{k \in \mathbb{N}} |\mu_{k+1} - \mu_k| < \infty$ to (A.7), we have $\lim_{k \rightarrow \infty} \|\mathbf{u}^{k+1} - \mathbf{u}^k\|_{\mathcal{M}} = 0$. Since $\mathbf{u}^{k+1} - \mathbf{u}^k = \mu_{k+1}(\mathbf{a} - \mathcal{T}\mathbf{u}^k)$, we have

$$(A.8) \quad \begin{aligned} \|\mathbf{u}^k - \mathcal{T}\mathbf{u}^k\|_{\mathcal{M}} &= \|(\mathbf{u}^k - \mathbf{u}^{k+1}) + (\mathbf{u}^{k+1} - \mathcal{T}\mathbf{u}^k)\|_{\mathcal{M}} \\ &\leq \|\mathbf{u}^k - \mathbf{u}^{k+1}\|_{\mathcal{M}} + \mu_{k+1} \|\mathbf{a} - \mathcal{T}\mathbf{u}^k\|_{\mathcal{M}}. \end{aligned}$$

Using (A.6) and $\lim_{k \rightarrow \infty} \mu_k = 0$ in (A.8), we can obtain $\lim_{k \rightarrow \infty} \|\mathbf{u}^k - \mathcal{T}\mathbf{u}^k\|_{\mathcal{M}} = 0$.

For (iii), let $M' = \|\mathbf{a} - \mathbf{u}^*\| + CC_1$, by the triangle inequality and (A.5), we have

$$(A.9) \quad \|\mathbf{a} - \mathcal{T}\mathbf{u}^k\| \leq \|\mathbf{a} - \mathbf{u}^*\| + \|\mathbf{u}^* - \mathcal{T}\mathbf{u}^k\| \leq \|\mathbf{a} - \mathbf{u}^*\| + CC_1 = M'.$$

Similar to the proof of (A.7), we have

$$(A.10) \quad \begin{aligned} \|\mathbf{u}^{k+1} - \mathbf{u}^k\| &\leq (1 - \mu_{k+1}) \|\mathcal{T}\mathbf{u}^k - \mathcal{T}\mathbf{u}^{k-1}\| + |\mu_{k+1} - \mu_k| \|\mathbf{a} - \mathcal{T}\mathbf{u}^{k-1}\| \\ &\leq C(1 - \mu_{k+1}) \|\mathbf{u}^k - \mathbf{u}^{k-1}\|_{\mathcal{M}} + M' |\mu_{k+1} - \mu_k|, \end{aligned}$$

where the last inequality follows from (A.3). Applying (A.7) and $\lim_{k \rightarrow \infty} \mu_k = 0$ to the above inequality (A.10), we have $\lim_{k \rightarrow \infty} \|\mathbf{u}^{k+1} - \mathbf{u}^k\| = 0$. Similar to the proof of (A.8),

$$\|\mathbf{u}^k - \mathcal{T}\mathbf{u}^k\| \leq \|\mathbf{u}^k - \mathbf{u}^{k+1}\| + \mu_{k+1} \|\mathbf{a} - \mathcal{T}\mathbf{u}^k\|.$$

By $\lim_{k \rightarrow \infty} \|\mathbf{u}^{k+1} - \mathbf{u}^k\| = 0$, $\lim_{k \rightarrow \infty} \mu_k = 0$ and boundedness of $\{\mathcal{T}\mathbf{u}^k\}_{k \in \mathbb{N}}$, we finally prove $\lim_{k \rightarrow \infty} \|\mathbf{u}^k - \mathcal{T}\mathbf{u}^k\| = 0$. \blacksquare

Appendix B. \mathcal{M} -projection.

Lemma B.1. *Let $\mathcal{A} : \mathcal{H} \rightarrow 2^{\mathcal{H}}$ be an operator with $\text{zer}\mathcal{A} \neq \emptyset$, and let \mathcal{M} be an admissible preconditioner such that $\mathcal{M}^{-1}\mathcal{A}$ is \mathcal{M} -monotone and $(\mathcal{M} + \mathcal{A})^{-1}$ is L -Lipschitz. Then there exists a unique solution $\mathbf{u}^* = \arg \min_{\mathbf{u} \in \text{Fix}(\mathcal{T})} \|\mathbf{u} - \mathbf{a}\|_{\mathcal{M}}^2$ which solves:*

$$\langle \mathbf{u}^* - \mathbf{a}, \mathbf{u} - \mathbf{u}^* \rangle_{\mathcal{M}} \geq 0 \quad \forall \mathbf{u} \in \text{Fix}(\mathcal{T}).$$

Proof. Since $l(\mathbf{u}) = \frac{1}{2} \|\mathbf{u} - \mathbf{a}\|_{\mathcal{M}}^2$ is a proper lower-semicontinuous differentiable convex function, assume that \mathbf{u}^* is the optimal solution of $\min_{\mathbf{u} \in \text{Fix}(\mathcal{T})} l(\mathbf{u})$. Since $\text{Fix}(\mathcal{T}) = \text{zer}\mathcal{A}$ is the convex set, thus $\mathbf{u}^* + t(\mathbf{u} - \mathbf{u}^*) \in \text{Fix}(\mathcal{T})$ for any $\mathbf{u} \in \text{Fix}(\mathcal{T})$ and $t \in (0, 1)$. Hence,

$$(B.1) \quad \begin{aligned} \lim_{t \rightarrow 0} \frac{l(\mathbf{u}^* + t(\mathbf{u} - \mathbf{u}^*)) - l(\mathbf{u}^*)}{t} &= \langle l'(\mathbf{u}^*), \mathbf{u} - \mathbf{u}^* \rangle \\ &= \langle \mathcal{M}(\mathbf{u}^* - \mathbf{a}), \mathbf{u} - \mathbf{u}^* \rangle \\ &= \langle \mathbf{u}^* - \mathbf{a}, \mathbf{u} - \mathbf{u}^* \rangle_{\mathcal{M}} \geq 0. \end{aligned}$$

If \mathbf{u}^{**} is the another solution, then it also satisfies

$$(B.2) \quad \langle \mathbf{u}^{**} - \mathbf{a}, \mathbf{u} - \mathbf{u}^{**} \rangle_{\mathcal{M}} \geq 0.$$

Replace \mathbf{u} with \mathbf{u}^{**} , \mathbf{u}^* in (B.1) and (B.2), respectively, then

$$\begin{aligned}\langle \mathbf{u}^* - \mathbf{a}, \mathbf{u}^{**} - \mathbf{u}^* \rangle_{\mathcal{M}} &\geq 0, \\ \langle \mathbf{u}^{**} - \mathbf{a}, \mathbf{u}^* - \mathbf{u}^{**} \rangle_{\mathcal{M}} &\geq 0.\end{aligned}$$

Add the above two inequalities, we then obtain $\|\mathbf{u}^* - \mathbf{u}^{**}\|_{\mathcal{M}} = 0$. By (A.3), we have

$$\|\mathbf{u}^* - \mathbf{u}^{**}\| = \|\mathcal{T}\mathbf{u}^* - \mathcal{T}\mathbf{u}^{**}\| \leq C \|\mathbf{u}^* - \mathbf{u}^{**}\|_{\mathcal{M}} = 0.$$

It follows $\mathbf{u}^* = \mathbf{u}^{**}$, which completes the proof of Lemma B.1. \blacksquare

As mentioned in [3, 15], we can introduce the following notion of \mathcal{M} -projection.

Definition B.2 (\mathcal{M} -projection). Assume $\mathbf{a} \in \mathcal{H}$ and that there exists a unique point $\mathbf{u}^* \in \text{Fix}(\mathcal{T})$ such that $\|\mathbf{u}^* - \mathbf{a}\|_{\mathcal{M}} \leq \|\mathbf{u} - \mathbf{a}\|_{\mathcal{M}}$ for any $\mathbf{u} \in \text{Fix}(\mathcal{T})$, then \mathbf{u}^* is called the \mathcal{M} -projection of \mathbf{a} onto $\text{Fix}(\mathcal{T})$, denoted by $P_{\text{Fix}(\mathcal{T})}^{\mathcal{M}}(\mathbf{a})$.

The following Lemma B.3 extends the variational inequality of the metric projection.

Lemma B.3. Let $\mathcal{A} : \mathcal{H} \rightarrow 2^{\mathcal{H}}$ be an operator with $\text{zer}\mathcal{A} \neq \emptyset$, and let \mathcal{M} be an admissible preconditioner such that $\mathcal{M}^{-1}\mathcal{A}$ is \mathcal{M} -monotone and $(\mathcal{M} + \mathcal{A})^{-1}$ is L -Lipschitz. Then the following assertions are equivalent:

- (i) $\mathbf{u}^* = P_{\text{Fix}(\mathcal{T})}^{\mathcal{M}}(\mathbf{a})$;
- (ii) $\langle \mathbf{u}^* - \mathbf{a}, \mathbf{u} - \mathbf{u}^* \rangle_{\mathcal{M}} \geq 0$ for any $\mathbf{u} \in \text{Fix}(\mathcal{T})$.

Proof. See Lemma B.1 and Definition B.2. \blacksquare

REFERENCES

- [1] R. AHMAD, C. A. BOUMAN, G. T. BUZZARD, S. CHAN, S. LIU, E. T. REEHORST, AND P. SCHNITER, *Plug-and-Play Methods for Magnetic Resonance Imaging: Using Denoisers for Image Recovery*, IEEE Signal Processing Magazine, 37 (2020), pp. 105–116, <https://doi.org/10.1109/MSP.2019.2949470>.
- [2] H. H. BAUSCHKE AND P. L. COMBETTES, *Convex Analysis and Monotone Operator Theory in Hilbert Spaces*, Springer Cham, second ed., 2017.
- [3] H. H. BAUSCHKE, W. M. MOURSI, S. SINGH, AND X. WANG, *On the Bredies-Chenchene-Lorenz-Naldi algorithm*, 2023, <https://arxiv.org/abs/2307.09747>.
- [4] H. H. BAUSCHKE, W. M. MOURSI, AND X. WANG, *Generalized monotone operators and their averaged resolvents*, Mathematical Programming, 189 (2021), pp. 55–74.
- [5] A. BECK, *First-order methods in optimization*, SIAM, 2017.
- [6] R. I. BOŦ AND D.-K. NGUYEN, *Fast Krasnosel’skiĭ–Mann Algorithm with a Convergence Rate of the Fixed Point Iteration of $\mathbf{o}(\frac{1}{k})$* , SIAM Journal on Numerical Analysis, 61 (2023), pp. 2813–2843.
- [7] R. I. BOŦ AND E. CHENCHENE, *Extra-Gradient Method with Flexible Anchoring: Strong Convergence and Fast Residual Decay*, 2024, <https://arxiv.org/abs/2410.14369>.
- [8] R. I. BOŦ AND D. MEIER, *A strongly convergent Krasnosel’skiĭ–Mann-type algorithm for finding a common fixed point of a countably infinite family of nonexpansive operators in Hilbert spaces*, Journal of Computational and Applied Mathematics, 395 (2021), p. 113589.
- [9] K. BREDIES, E. CHENCHENE, D. A. LORENZ, AND E. NALDI, *Degenerate Preconditioned Proximal Point Algorithms*, SIAM Journal on Optimization, 32 (2022), pp. 2376–2401, <https://doi.org/10.1137/21M1448112>.
- [10] K. BREDIES, J. CHIRINOS-RODRIGUEZ, AND E. NALDI, *Learning Firmly Nonexpansive Operators*, 2024, <https://arxiv.org/abs/2407.14156>.

-
- [11] K. BREDIES AND H. SUN, *Preconditioned Douglas–Rachford Splitting Methods for Convex-concave Saddle-point Problems*, SIAM Journal on Numerical Analysis, 53 (2015), pp. 421–444, <https://doi.org/10.1137/140965028>.
- [12] K. BREDIES AND H. SUN, *A Proximal Point Analysis of the Preconditioned Alternating Direction Method of Multipliers*, Journal of Optimization Theory and Applications, 173 (2017), pp. 878–907, <https://doi.org/10.1007/s10957-017-1112-5>.
- [13] M. N. BÙI AND P. L. COMBETTES, *The Douglas–Rachford Algorithm Converges Only Weakly*, SIAM Journal on Control and Optimization, 58 (2020), pp. 1118–1120, <https://doi.org/10.1137/19M1308451>.
- [14] G. T. BUZZARD, S. H. CHAN, S. SREEHARI, AND C. A. BOUMAN, *Plug-and-Play Unplugged: Optimization-Free Reconstruction Using Consensus Equilibrium*, SIAM Journal on Imaging Sciences, 11 (2018), pp. 2001–2020, <https://doi.org/10.1137/17M1122451>.
- [15] M. N. BÙI AND P. L. COMBETTES, *Warped proximal iterations for monotone inclusions*, Journal of Mathematical Analysis and Applications, 491 (2020), p. 124315, <https://www.sciencedirect.com/science/article/pii/S0022247X20304777>.
- [16] A. CHAMBOLLE AND T. POCK, *A First-Order Primal-Dual Algorithm for Convex Problems with Applications to Imaging*, Journal of Mathematical Imaging and Vision, 40 (2011), pp. 120–145, <https://doi.org/10.1007/s10851-010-0251-1>.
- [17] K. CHEN, D. SUN, Y. YUAN, G. ZHANG, AND X. ZHAO, *HPR-LP: An implementation of an HPR method for solving linear programming*, 2024, <https://arxiv.org/abs/2408.12179>.
- [18] Y. CHEN AND T. POCK, *Trainable Nonlinear Reaction Diffusion: A Flexible Framework for Fast and Effective Image Restoration*, IEEE Transactions on Pattern Analysis and Machine Intelligence, 39 (2017), pp. 1256–1272, <https://doi.org/10.1109/TPAMI.2016.2596743>.
- [19] R. COHEN, Y. BLAU, D. FREEDMAN, AND E. RIVLIN, *It Has Potential: Gradient-Driven Denoisers for Convergent Solutions to Inverse Problems*, in Advances in Neural Information Processing Systems, vol. 34, Curran Associates, Inc., 2021, pp. 18152–18164.
- [20] R. COHEN, M. ELAD, AND P. MILANFAR, *Regularization by Denoising via Fixed-Point Projection (RED-PRO)*, SIAM Journal on Imaging Sciences, 14 (2021), pp. 1374–1406.
- [21] B. DELATTRE, Q. BARTHÉLEMY, A. ARAUJO, AND A. ALLAUZEN, *Efficient bound of Lipschitz constant for convolutional layers by Gram iteration*, in Proceedings of the 40th International Conference on Machine Learning, vol. 202 of Proceedings of Machine Learning Research, PMLR, 23–29 Jul 2023, pp. 7513–7532.
- [22] J. DIAKONIKOLAS, *Halpern Iteration for Near-Optimal and Parameter-Free Monotone Inclusion and Strong Solutions to Variational Inequalities*, in Proceedings of Thirty Third Conference on Learning Theory, vol. 125 of Proceedings of Machine Learning Research, PMLR, 09–12 Jul 2020, pp. 1428–1451.
- [23] J. ECKSTEIN AND D. P. BERTSEKAS, *On the Douglas–Rachford splitting method and the proximal point algorithm for maximal monotone operators*, Mathematical Programming, 55 (1992), pp. 293–318, <https://doi.org/10.1007/BF01581204>.
- [24] H. W. ENGL, M. HANKE, AND A. NEUBAUER, *Regularization of inverse problems*, vol. 375, Springer Science & Business Media, 1996.
- [25] R. GRIBONVAL AND M. NIKOLOVA, *A Characterization of Proximity Operators*, Journal of Mathematical Imaging and Vision, 62 (2020), pp. 773–789, <https://doi.org/10.1007/s10851-020-00951-y>.
- [26] B. HALPERN, *Fixed points of nonexpanding maps*, Bulletin of the American Mathematical Society, 73 (1967), pp. 957–961.
- [27] B. HE AND X. YUAN, *Convergence Analysis of Primal-Dual Algorithms for a Saddle-Point Problem: From Contraction Perspective*, SIAM Journal on Imaging Sciences, 5 (2012), pp. 119–149, <https://doi.org/10.1137/100814494>.
- [28] B. HE AND X. YUAN, *On the convergence rate of Douglas–Rachford operator splitting method*, Mathematical Programming, 153 (2015), pp. 715–722, <https://doi.org/10.1007/s10107-014-0805-x>.
- [29] S. HE, H.-K. XU, Q.-L. DONG, AND N. MEI, *Convergence analysis of the Halpern iteration with adaptive anchoring parameters*, Mathematics of Computation, 93 (2024), pp. 327–345.
- [30] X. U. HONG-KUN, *Iterative Algorithms for Nonlinear Operators*, Journal of the London Mathematical Society, 66 (2002), pp. 240–256.
- [31] H. S. HUNDAL, *An alternating projection that does not converge in norm*, Nonlinear Analysis: Theory, Methods & Applications, 57 (2004), pp. 35–61, <https://doi.org/https://doi.org/10.1016/j.na.2003.11>.

- 004.
- [32] S. HURAUULT, A. LECLAIRE, AND N. PAPADAKIS, *Gradient Step Denoiser for convergent Plug-and-Play*, in International Conference on Learning Representations, 2022.
 - [33] S. HURAUULT, A. LECLAIRE, AND N. PAPADAKIS, *Proximal Denoiser for Convergent Plug-and-Play Optimization with Nonconvex Regularization*, in Proceedings of the 39th International Conference on Machine Learning, vol. 162 of Proceedings of Machine Learning Research, PMLR, 17–23 Jul 2022, pp. 9483–9505, <https://proceedings.mlr.press/v162/hurault22a.html>.
 - [34] C. IZUCHUKWU, S. REICH, Y. SHEHU, AND A. TAIWO, *Strong Convergence of Forward-Reflected-Backward Splitting Methods for Solving Monotone Inclusions with Applications to Image Restoration and Optimal Control*, Journal of Scientific Computing, 94 (2023), p. 73, <https://doi.org/10.1007/s10915-023-02132-6>.
 - [35] U. S. KAMILOV, C. A. BOUMAN, G. T. BUZZARD, AND B. WOHLBERG, *Plug-and-Play Methods for Integrating Physical and Learned Models in Computational Imaging: Theory, algorithms, and applications*, IEEE Signal Processing Magazine, 40 (2023), pp. 85–97, <https://doi.org/10.1109/MSP.2022.3199595>.
 - [36] F. LIEDER, *On the convergence rate of the Halpern-iteration*, Optimization letters, 15 (2021), pp. 405–418.
 - [37] P.-L. LIONS, *Approximation de points fixes de contractions*, CR Acad. Sci. Paris Serie, AB, 284 (1977), pp. 1357–1359.
 - [38] H. LU AND J. YANG, *Restarted Halpern PDHG for Linear Programming*, 2024, <https://arxiv.org/abs/2407.16144>.
 - [39] G. J. MINTY, *Monotone (nonlinear) operators in hilbert space*, Duke Mathematical Journal, 29 (1962), pp. 341–346, <https://api.semanticscholar.org/CorpusID:121956938>.
 - [40] J.-J. MOREAU, *Proximité et dualité dans un espace hilbertien*, Bulletin de la Société mathématique de France, 93 (1965), pp. 273–299.
 - [41] J. PARK AND E. K. RYU, *Exact Optimal Accelerated Complexity for Fixed-Point Iterations*, in Proceedings of the 39th International Conference on Machine Learning, vol. 162 of Proceedings of Machine Learning Research, PMLR, 17–23 Jul 2022, pp. 17420–17457.
 - [42] J.-C. PESQUET, A. REPETTI, M. TERRIS, AND Y. WIAUX, *Learning Maximally Monotone Operators for Image Recovery*, SIAM Journal on Imaging Sciences, 14 (2021), pp. 1206–1237, <https://doi.org/10.1137/20M1387961>.
 - [43] T. POCK AND A. CHAMBOLLE, *Diagonal preconditioning for first order primal-dual algorithms in convex optimization*, in 2011 International Conference on Computer Vision, 2011, pp. 1762–1769, <https://doi.org/10.1109/ICCV.2011.6126441>.
 - [44] H. QI AND H.-K. XU, *Convergence of Halpern’s Iteration Method with Applications in Optimization*, Numerical Functional Analysis and Optimization, 42 (2021), pp. 1839–1854.
 - [45] E. T. REEHORST AND P. SCHNITER, *Regularization by Denoising: Clarifications and New Interpretations*, IEEE Transactions on Computational Imaging, 5 (2019), pp. 52–67, <https://doi.org/10.1109/TCI.2018.2880326>.
 - [46] R. T. ROCKAFELLAR, *Monotone Operators and the Proximal Point Algorithm*, SIAM Journal on Control and Optimization, 14 (1976), pp. 877–898.
 - [47] Y. ROMANO, M. ELAD, AND P. MILANFAR, *The Little Engine That Could: Regularization by Denoising (RED)*, SIAM Journal on Imaging Sciences, 10 (2017), pp. 1804–1844, <https://doi.org/10.1137/16M1102884>.
 - [48] L. I. RUDIN, S. OSHER, AND E. FATEMI, *Nonlinear total variation based noise removal algorithms*, Physica D: Nonlinear Phenomena, 60 (1992), pp. 259–268, <https://www.sciencedirect.com/science/article/pii/016727899290242F>.
 - [49] E. RYU, J. LIU, S. WANG, X. CHEN, Z. WANG, AND W. YIN, *Plug-and-Play Methods Provably Converge with Properly Trained Denoisers*, in International Conference on Machine Learning, PMLR, 2019, pp. 5546–5557.
 - [50] S. SABACH AND S. SHTERN, *A First Order Method for Solving Convex Bilevel Optimization Problems*, SIAM Journal on Optimization, 27 (2017), pp. 640–660, <https://doi.org/10.1137/16M105592X>.
 - [51] S. SREEHARI, S. V. VENKATAKRISHNAN, B. WOHLBERG, G. T. BUZZARD, L. F. DRUMMY, J. P. SIMMONS, AND C. A. BOUMAN, *Plug-and-Play Priors for Bright Field Electron Tomography and Sparse Interpolation*, IEEE Transactions on Computational Imaging, 2 (2016), pp. 408–423, <https://doi.org/10.1109/TCI.2016.2599778>.

-
- [52] D. SUN, Y. YUAN, G. ZHANG, AND X. ZHAO, *Accelerating preconditioned admm via degenerate proximal point mappings*, SIAM Journal on Optimization, 35 (2025), pp. 1165–1193, <https://doi.org/10.1137/24M1650053>.
- [53] H. Y. TAN, S. MUKHERJEE, J. TANG, AND C.-B. SCHÖNLIEB, *Provably Convergent Plug-and-Play Quasi-Newton Methods*, SIAM Journal on Imaging Sciences, 17 (2024), pp. 785–819, <https://doi.org/10.1137/23M157185X>.
- [54] M. TERRIS, A. REPETTI, J.-C. PESQUET, AND Y. WIAUX, *Building Firmly Nonexpansive Convolutional Neural Networks*, in ICASSP 2020 - 2020 IEEE International Conference on Acoustics, Speech and Signal Processing (ICASSP), 2020, pp. 8658–8662, <https://doi.org/10.1109/ICASSP40776.2020.9054731>.
- [55] Q. TRAN-DINH, *From Halpern's fixed-point iterations to Nesterov's accelerated interpretations for root-finding problems*, Computational Optimization and Applications, 87 (2024), pp. 181–218, <https://doi.org/10.1007/s10589-023-00518-8>.
- [56] S. V. VENKATAKRISHNAN, C. A. BOUMAN, AND B. WOHLBERG, *Plug-and-Play priors for model based reconstruction*, in 2013 IEEE Global Conference on Signal and Information Processing, 2013, pp. 945–948, <https://doi.org/10.1109/GlobalSIP.2013.6737048>.
- [57] D. WEI, P. CHEN, AND F. LI, *Learning Pseudo-Contractive Denoisers for Inverse Problems*, in Proceedings of the 41st International Conference on Machine Learning, vol. 235 of Proceedings of Machine Learning Research, PMLR, 21–27 Jul 2024, pp. 52500–52524.
- [58] R. WITTMANN, *Approximation of fixed points of nonexpansive mappings*, Archiv der Mathematik, 58 (1992), pp. 486–491, <https://doi.org/10.1007/BF01190119>.
- [59] Z. WU, C. HUANG, AND T. ZENG, *Extrapolated Plug-and-Play Three-Operator Splitting Methods for Nonconvex Optimization with Applications to Image Restoration*, SIAM Journal on Imaging Sciences, 17 (2024), pp. 1145–1181, <https://doi.org/10.1137/23M1611166>.
- [60] Z. WU, Y. SUN, Y. CHEN, B. ZHANG, Y. YUE, AND K. BOUMAN, *Principled Probabilistic Imaging using Diffusion Models as Plug-and-Play Priors*, in Advances in Neural Information Processing Systems, vol. 37, Curran Associates, Inc., 2024, pp. 118389–118427.
- [61] H.-K. XU, *Viscosity approximation methods for nonexpansive mappings*, Journal of Mathematical Analysis and Applications, 298 (2004), pp. 279–291.
- [62] F. XUE, *A generalized forward-backward splitting operator: degenerate analysis and applications*, Computational and Applied Mathematics, 42 (2023), <https://doi.org/10.1007/s40314-022-02143-3>.
- [63] I. YAMADA, *The hybrid steepest descent method for the variational inequality problem over the intersection of fixed point sets of nonexpansive mappings*, Inherently parallel algorithms in feasibility and optimization and their applications, 8 (2001), pp. 473–504.
- [64] I. YAMADA AND N. OGURA, *Hybrid Steepest Descent Method for Variational Inequality Problem over the Fixed Point Set of Certain Quasi-nonexpansive Mappings*, Numerical Functional Analysis and Optimization, 25 (2005), pp. 619–655, <https://doi.org/10.1081/NFA-200045815>.
- [65] K. ZHANG, Y. LI, W. ZUO, L. ZHANG, L. VAN GOOL, AND R. TIMOFTE, *Plug-and-play image restoration with deep denoiser prior*, IEEE Transactions on Pattern Analysis and Machine Intelligence, 44 (2022), pp. 6360–6376, <https://doi.org/10.1109/TPAMI.2021.3088914>.
- [66] K. ZHANG, W. ZUO, Y. CHEN, D. MENG, AND L. ZHANG, *Beyond a Gaussian Denoiser: Residual Learning of Deep CNN for Image Denoising*, IEEE Transactions on Image Processing, 26 (2017), pp. 3142–3155, <https://doi.org/10.1109/TIP.2017.2662206>.